

inhibited LV remodeling and failure after MI.¹³ However, GSHPx is located predominantly in the cytosol, and only a small proportion ($\approx 10\%$) is present in the mitochondria.²⁰ Therefore, it remains unclear whether the beneficial effects of GSHPx overexpression on post-MI hearts were attributable to an increase of this enzyme in the cytosol, the mitochondria, or both. The specific localization of Prx-3 in the mitochondria suggests that mitochondrial oxidative stress plays an important role in the development and progression of heart failure, and antioxidants localized specifically within the mitochondria provide a primary line of defense against this disease process.

A growing body of evidence suggests that ROS play a major role in the pathogenesis of cardiac failure. Furthermore, antioxidants have been shown to exert protective and beneficial effects against heart failure.^{21,22} A previous study from our laboratory demonstrated that dimethylthiourea improved survival and prevented LV remodeling and failure after MI.¹⁰ However, the most effective way to evaluate the contribution of any specific antioxidant and obtain direct evidence of an adverse role for ROS in heart failure is through gene manipulation. Therefore, the present study not only extends the previous observation that used antioxidants but also reveals the major role of mitochondrial oxidative stress in the pathophysiology of post-MI remodeling and failure.

The beneficial effects of Prx-3 overexpression shown in the present study were not due to its MI size-sparing effect, because there was no statistically significant difference in infarct size between WT+MI and TG+MI mice. Furthermore, its effects were not attributable to hemodynamics because blood pressures and heart rates were not altered (Table 1). Importantly, it is also unlikely that these effects were caused by the altered expression of antioxidant enzymes other than Prx-3 (Table 1). Moreover, the beneficial effects of Prx-3 overexpression were not due to systemic induction of antioxidant defenses. This possibility is less likely because plasma TBARS were comparable between WT+MI and TG+MI mice. Nevertheless, we cannot completely exclude the possibility that the systemic effects of Prx-3 induction might also have contributed to this phenotype because this TG is not heart-specific.

There may be several factors contributing to the protective effects conferred by Prx-3 overexpression on post-MI remodeling and failure. First, recent studies have demonstrated that a Trx-related antioxidant system is closely associated with the regulation of apoptosis, probably through quenching of ROS and redox control of the mitochondrial permeability transition pores that release cytochrome *c*.²³ A subtle increase in ROS caused by partial inhibition of SOD results in apoptosis in isolated cardiac myocytes.²⁴ Previous studies have demonstrated that apoptosis appears not only in infarcted but also in noninfarcted myocardium after MI.²⁵ Specifically, apoptosis occurs in the noninfarcted LV late after MI. This is an intriguing observation, in light of the remodeling process known to occur within the noninfarcted area, which is characterized by the loss of myocytes and hypertrophy. In fact, recent studies have suggested cardiac myocyte apoptosis contributes to LV remodeling after MI.^{26,27} Importantly, increased oxidative stress occurs concomitantly with in-

creased cardiac myocyte apoptosis within the noninfarcted area. This is a provoking observation, because oxidative stress is a powerful inducer of apoptotic cell death.²⁸ The present study suggests that the coexistence of oxidative stress and myocyte apoptosis in the noninfarcted LV after MI is causally related. Oxidative stress may mediate myocyte apoptosis, which may lead to myocardial remodeling and failure. Therefore, the decreased mitochondrial oxidative stress due to Prx-3 overexpression could contribute to the amelioration of apoptosis (Figure 5) and eventual post-MI cardiac failure. Second, Prx-3 overexpression prevented the decrease in mtDNA copy number (Figure 6) as well as mitochondrial complex enzyme activities (Table 2). Our previous studies have demonstrated an intimate link between mtDNA damage, increased lipid peroxidation, and a decrease in mitochondrial function, which might play a major role in the development and progression of cardiac failure.⁴

There are several issues to be acknowledged as limitations of this study. First, the differences between WT+MI and TG+MI groups in their echocardiographic measurements are not remarkable, even though they are statistically significant (Table 1). However, our previous study showed that the intraobserver and interobserver variabilities in our echocardiographic measurements for LV dimensions were small, and measurements made in the same animals on separate days were highly reproducible.¹² Therefore, these values are considered to be valid. Second, longer-term follow-up data are not available for the animals in the current study. We therefore could not determine whether the differences between WT+MI and TG+MI groups seen in the present study were more or less significant at later time points, when additional LV remodeling would have been expected to occur.

In conclusion, Prx-3 overexpression inhibited the development of LV remodeling and failure after MI, which was associated with an attenuation of myocyte hypertrophy, apoptosis, and interstitial fibrosis. It also ameliorated mitochondrial oxidative stress as well as mtDNA decline and mitochondrial dysfunction in post-MI hearts. Therapies designed to interfere with mitochondrial oxidative stress could be beneficial to prevent heart failure after MI.

Acknowledgments

This study was supported in part by grants from the Ministry of Education, Science and Culture (No. 12670676, 14370230, 17390223). A portion of this study was conducted at Kyushu University Station for Collaborative Research I and II.

Disclosures

None.

References

- Ide T, Tsutsui H, Kinugawa S, Suematsu N, Hayashidani S, Ichikawa K, Utsumi H, Machida Y, Egashira K, Takeshita A. Direct evidence for increased hydroxyl radicals originating from superoxide in the failing myocardium. *Circ Res*. 2000;86:152–157.
- Mallat Z, Philip I, Lebre M, Chatel D, Maclouf J, Tedgui A. Elevated levels of 8-iso-prostaglandin F₂ α in pericardial fluid of patients with heart failure: a potential role for in vivo oxidant stress in ventricular dilatation and progression to heart failure. *Circulation*. 1998;97:1536–1539.

3. Ide T, Tsutsui H, Kinugawa S, Utsumi H, Kang D, Hattori N, Uchida K, Arimura K, Egashira K, Takeshita A. Mitochondrial electron transport complex I is a potential source of oxygen free radicals in the failing myocardium. *Circ Res*. 1999;85:357–363.
4. Ide T, Tsutsui H, Hayashidani S, Kang D, Suematsu N, Nakamura K, Utsumi H, Hamasaki N, Takeshita A. Mitochondrial DNA damage and dysfunction associated with oxidative stress in failing hearts after myocardial infarction. *Circ Res*. 2001;88:529–535.
5. Suematsu N, Tsutsui H, Wen J, Kang D, Ikeuchi M, Ide T, Hayashidani S, Shiomi T, Kubota T, Hamasaki N, Takeshita A. Oxidative stress mediates tumor necrosis factor- α -induced mitochondrial DNA damage and dysfunction in cardiac myocytes. *Circulation*. 2003;107:1418–1423.
6. Bryk R, Griffin P, Nathan C. Peroxynitrite reductase activity of bacterial peroxiredoxins. *Nature*. 2000;407:211–215.
7. Kang SW, Chae HZ, Seo MS, Kim K, Baines IC, Rhee SG. Mammalian peroxiredoxin isoforms can reduce hydrogen peroxide generated in response to growth factors and tumor necrosis factor- α . *J Biol Chem*. 1998;273:6297–6302.
8. Hattori F, Murayama N, Noshita T, Oikawa S. Mitochondrial peroxiredoxin-3 protects hippocampal neurons from excitotoxic injury in vivo. *J Neurochem*. 2003;86:860–868.
9. Sia YT, Lapointe N, Parker TG, Tsoporis JN, Deschepper CF, Calderone A, Pourjabbar A, Jasmin JF, Sarrazin JF, Liu P, Adam A, Butany J, Rouleau JL. Beneficial effects of long-term use of the antioxidant probucol in heart failure in the rat. *Circulation*. 2002;105:2549–2555.
10. Kinugawa S, Tsutsui H, Hayashidani S, Ide T, Suematsu N, Satoh S, Utsumi H, Takeshita A. Treatment with dimethylthiourea prevents left ventricular remodeling and failure after experimental myocardial infarction in mice: role of oxidative stress. *Circ Res*. 2000;87:392–398.
11. Ho YS, Magnenat JL, Bronson RT, Cao J, Gargano M, Sugawara M, Funk CD. Mice deficient in cellular glutathione peroxidase develop normally and show no increased sensitivity to hyperoxia. *J Biol Chem*. 1997;272:16644–16651.
12. Shiomi T, Tsutsui H, Hayashidani S, Suematsu N, Ikeuchi M, Wen J, Ishibashi M, Kubota T, Egashira K, Takeshita A. Pioglitazone, a peroxisome proliferator-activated receptor- γ agonist, attenuates left ventricular remodeling and failure after experimental myocardial infarction. *Circulation*. 2002;106:3126–3132.
13. Shiomi T, Tsutsui H, Matsusaka H, Murakami K, Hayashidani S, Ikeuchi M, Wen J, Kubota T, Utsumi H, Takeshita A. Overexpression of glutathione peroxidase prevents left ventricular remodeling and failure after myocardial infarction in mice. *Circulation*. 2004;109:544–549.
14. Ide T, Tsutsui H, Ohashi N, Hayashidani S, Suematsu N, Tsuchihashi M, Tamai H, Takeshita A. Greater oxidative stress in healthy young men compared with premenopausal women. *Arterioscler Thromb Vasc Biol*. 2002;22:438–442.
15. Wood ZA, Schroder E, Robin Harris J, Poole LB. Structure, mechanism and regulation of peroxiredoxins. *Trends Biochem Sci*. 2003;28:32–40.
16. Fisher AB, Dodia C, Manevich Y, Chen JW, Feinstein SI. Phospholipid hydroperoxides are substrates for non-selenium glutathione peroxidase. *J Biol Chem*. 1999;274:21326–21334.
17. Watabe S, Hiroi T, Yamamoto Y, Fujioka Y, Hasegawa H, Yago N, Takahashi SY. SP-22 is a thioredoxin-dependent peroxide reductase in mitochondria. *Eur J Biochem*. 1997;249:52–60.
18. Nonn L, Berggren M, Powis G. Increased expression of mitochondrial peroxiredoxin-3 (thioredoxin peroxidase-2) protects cancer cells against hypoxia and drug-induced hydrogen peroxide-dependent apoptosis. *Mol Cancer Res*. 2003;1:682–689.
19. Banmeyer I, Marchand C, Clippe A, Knoop B. Human mitochondrial peroxiredoxin 5 protects from mitochondrial DNA damages induced by hydrogen peroxide. *FEBS Lett*. 2005;579:2327–2333.
20. Chang TS, Cho CS, Park S, Yu S, Kang SW, Rhee SG. Peroxiredoxin III, a mitochondrion-specific peroxidase, regulates apoptotic signaling by mitochondria. *J Biol Chem*. 2004;279:41975–41984.
21. Dhalla AK, Hill MF, Singal PK. Role of oxidative stress in transition of hypertrophy to heart failure. *J Am Coll Cardiol*. 1996;28:506–514.
22. Nakamura R, Egashira K, Machida Y, Hayashidani S, Takeya M, Utsumi H, Tsutsui H, Takeshita A. Probucol attenuates left ventricular dysfunction and remodeling in tachycardia-induced heart failure: roles of oxidative stress and inflammation. *Circulation*. 2002;106:362–367.
23. Petronilli V, Costantini P, Scorrano L, Colonna R, Passamonti S, Bernardi P. The voltage sensor of the mitochondrial permeability transition pore is tuned by the oxidation-reduction state of vicinal thiols: increase of the gating potential by oxidants and its reversal by reducing agents. *J Biol Chem*. 1994;269:16638–16642.
24. Siwik DA, Tzortzis JD, Pimental DR, Chang DL, Pagano PJ, Singh K, Sawyer DB, Colucci WS. Inhibition of copper-zinc superoxide dismutase induces cell growth, hypertrophic phenotype, and apoptosis in neonatal rat cardiac myocytes in vitro. *Circ Res*. 1999;85:147–153.
25. Palojoki E, Saraste A, Eriksson A, Pulkki K, Kallajoki M, Voipio-Pulkki LM, Tikkanen I. Cardiomyocyte apoptosis and ventricular remodeling after myocardial infarction in rats. *Am J Physiol Heart Circ Physiol*. 2001;280:H2726–H2731.
26. Sam F, Sawyer DB, Chang DL, Eberli FR, Ngoy S, Jain M, Amin J, Apstein CS, Colucci WS. Progressive left ventricular remodeling and apoptosis late after myocardial infarction in mouse heart. *Am J Physiol Heart Circ Physiol*. 2000;279:H422–H428.
27. Oskarsson HJ, Coppey L, Weiss RM, Li WG. Antioxidants attenuate myocyte apoptosis in the remote non-infarcted myocardium following large myocardial infarction. *Cardiovasc Res*. 2000;45:679–687.
28. von Harsdorf R, Li PF, Dietz R. Signaling pathways in reactive oxygen species-induced cardiomyocyte apoptosis. *Circulation*. 1999;99:2934–2941.

CLINICAL PERSPECTIVE

A growing body of evidence suggests that oxidative stress, an excess generation of reactive oxygen species (ROS), plays a major role in the pathogenesis of heart failure. Furthermore, antioxidants have been shown to exert protective and beneficial effects against this process. Recent studies have suggested that mitochondria are the predominant source of ROS in the failing heart, and mitochondrial antioxidants are expected to be the first line of defense against mitochondrial oxidative stress-mediated myocardial injury. The present study demonstrated that overexpression of peroxiredoxin-3 (Prx-3) inhibited cardiac remodeling and failure after myocardial infarction (MI) created by ligation of the left coronary artery in mice. Prx-3 contains a mitochondrial localization sequence, is found exclusively in the mitochondria, and uses mitochondrial thioredoxin (Trx)-2 as the electron donor for its peroxidase activity. It functions not only by removing H₂O₂ formed after the superoxide dismutase (SOD)-catalyzed dismutation reaction but also by detoxifying peroxynitrite. Therefore, the great efficiency of Prx-3 as an antioxidant shown in the present study may be attributable to the fact that it is located in the mitochondria and can utilize lipid peroxides as well as H₂O₂ for substrates. The present study not only extends previous investigations that used antioxidants but also reveals a major role for mitochondrial oxidative stress in the pathophysiology of postinfarct heart failure. Therapies designed to interfere with mitochondrial oxidative stress by using antioxidant Prx-3 might also be beneficial in preventing clinical heart failure.



ELSEVIER

Cardiovascular Research 70 (2006) 457–465

Cardiovascular
Research

www.elsevier.com/locate/cardiore

Targeted deletion of p53 prevents cardiac rupture after myocardial infarction in mice

Hidenori Matsusaka^a, Tomomi Ide^a, Shouji Matsushima^a, Masaki Ikeuchi^a, Toru Kubota^a,
Kenji Sunagawa^a, Shintaro Kinugawa^b, Hiroyuki Tsutsui^{b,*}

^a Department of Cardiovascular Medicine, Graduate School of Medical Sciences, Kyushu University, Fukuoka 812-8582, Japan

^b Department of Cardiovascular Medicine, Hokkaido University Graduate School of Medicine, Kita-15, Nishi-7, Kita-ku, Sapporo 060-8638, Japan

Received 10 August 2005; received in revised form 23 January 2006; accepted 1 February 2006

Available online 13 March 2006

Time for primary review 43 days

Abstract

Objective: Apoptosis may play an important role in cardiac remodeling after myocardial infarction (MI). p53 is a well-known proapoptotic factor. However, its pathophysiological significance in these conditions remains unclear. We thus examined the effects of target deletion of the p53 gene on post-MI hearts.

Methods: Anterior MI was created in male heterozygous p53-deficient (p53^{+/-}; n=28) mice and sibling wild-type (p53^{+/+}; n=29) mice by ligating the left coronary artery.

Results: By day 7, p53^{+/-} mice had significantly better survival rate than p53^{+/+} mice (89% vs. 69%, $P<0.05$). Notably, p53^{+/-} mice had a significantly lower incidence of left ventricular (LV) rupture (7% vs. 28%, $P<0.05$) despite comparable infarct size (60±2% vs. 59±2%, $P=NS$), heart rate (488±15 vs. 489±17 bpm, $P=NS$), or mean arterial blood pressure (80±2 vs. 78±3 mm Hg, $P=NS$). The extent of infiltrating interstitial cells including macrophages into the post-MI hearts was not altered by the deletion of p53. Further, collagen deposition as well as the zymographic MMP-2 and -9 activities were comparable between p53^{+/-} and p53^{+/+} mice with MI. However, the p53^{+/-} mice had a significantly thicker infarct wall. The number of TUNEL-positive cells in the infarct area was significantly lower in p53^{+/-} mice than in p53^{+/+} mice (423±86 vs. 1330±275/10⁵ cells, $P<0.01$).

Conclusions: p53 is involved in cardiac rupture after MI, probably via the induction of a proapoptotic pathway. The inhibition of p53 may be a potentially useful therapeutic strategy to manage post-MI patients.

© 2006 European Society of Cardiology. Published by Elsevier B.V. All rights reserved.

Keywords: Apoptosis; Extracellular matrix; Infarction; Myocytes; Remodeling

This article is referred to in the Editorial by M.T. Crow (pages 401–403) in this issue.

1. Introduction

Myocardial infarction (MI) leads to complex structural alterations (remodeling) involving both the infarcted and noninfarcted left ventricular (LV) myocardium [1]. Early remodeling, which occurs during the early phase of MI, is

characteristic for LV wall thinning and cavity dilatation in the infarct region (infarct expansion). Cardiac rupture is a lethal complication accounting for 5–30% of in-hospital mortality of MI [2] and is often associated with a transmural infarction, no prior history of angina pectoris, and a relatively large Q-wave infarct. Although the significance of these factors remains unestablished, accumulated lines of evidence have suggested that cardiac rupture results from the continuous stretch of infarcted and structurally weakened myocardium [3]. Recently, inflammatory cell infiltration and activation of matrix metalloproteinases (MMPs) have also been implicated in the pathogenesis of cardiac rupture [4,5].

* Corresponding author. Tel.: +81 11 706 6970; fax: +81 11 706 7874.
E-mail address: htsutsui@med.hokudai.ac.jp (H. Tsutsui).

The tumor suppressor gene p53 is an important transcription factor regulating cell death and proliferation. It induces apoptosis in response to a variety of stresses such as ischemia [6,7]. In fact, there is evidence supporting that p53 is activated in the ischemic hearts [8] and apoptotic myocytes are detected in the infarcted and border zone regions during the early days of MI [9,10]. Based on these lines of evidence, we postulated that p53-dependent apoptosis might play an important role in early LV rupture after MI. However, no previous studies have yet determined the pathophysiological significance of p53 in this deleterious process. In the present study, we evaluated the effects of a targeted deletion of the p53 gene on the development of cardiac apoptosis and rupture after experimental MI in mice. To ensure selective and long-term complete inhibition of p53, we employed p53 knockout mice [11] because the most effective way to obtain the direct evidence for a role of p53 is through gene manipulation. We demonstrated that p53 was involved in cardiac rupture after MI, probably via the induction of proapoptotic pathway. The inhibition of p53 may be a potentially useful therapeutic strategy to manage post-MI patients.

2. Methods

2.1. Animals

The study was approved by our Institutional Animal Research Committee and conformed with the *Guide for the Care and Use of Laboratory Animals* published by the US National Institutes of Health (NIH Publication No. 85-23, revised 1996). We used the progeny of homozygous p53 deficient mice ($p53^{-/-}$), heterozygous p53 deficient mice ($p53^{+/-}$), and their wild-type littermates ($p53^{+/+}$, C57BL/6J) ranging in age from 10 to 14 weeks old. $p53^{-/-}$ and $p53^{+/-}$ mice are viable, fertile, and indistinguishable from $p53^{+/+}$ mice in appearance but are prone to the spontaneous development of a variety of tumors by 6 months of age [12]. We thus assessed mice at the age of 10 to 14 weeks old for comparison between groups. The original breeding pairs used to develop the mice for this study were obtained from Jackson Laboratories (Bar Harbor, Maine). Genotypes of the mice were determined by PCR analyses of the mouse tail DNAs [13]. For p53, we used a sense oligonucleotide primer (5'-CCCGAGTATCTGGAAGACAG-3') and an antisense primer (5'-ATAGGTCGGCGGTTTCAT-3'). For the neomycin cassette, we also used a sense oligonucleotide primer (5'-CTTGGGTGGAGAGGCTATTC-3') and an antisense primer (5'-AGGTGAGATGACAGGAGATC-3'). The amplicon from the WT allele is 600 bp, and the mutant allele is 280 bp (Fig. 1).

2.2. Creation of MI

We created MI in male $p53^{-/-}$ ($p53^{-/-}$ +MI), $p53^{+/-}$ ($p53^{+/-}$ +MI), and sibling wild-type mice ($p53^{+/+}$ +MI) by

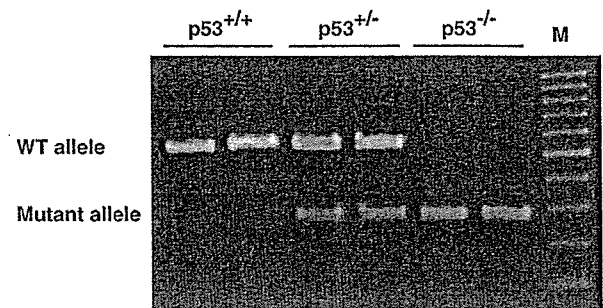


Fig. 1. PCR genotyping of $p53^{+/+}$, $p53^{+/-}$, and $p53^{-/-}$ mice. The amplicon from the WT allele is 600 bp, and the mutant allele is 280 bp. M, marker.

ligating the left coronary artery [14]. A sham operation without coronary artery ligation was also performed in both $p53^{+/+}$ ($p53^{+/+}$ +Sham) and $p53^{+/-}$ ($p53^{+/-}$ +Sham) mice.

2.3. Experimental protocol 1: 7-day post-MI study

2.3.1. Survival

A survival analysis was performed for the $p53^{+/+}$ +MI ($n=29$), $p53^{+/-}$ +MI ($n=28$), and $p53^{-/-}$ +MI ($n=20$) mice. During the 7-day study period, the cages were inspected daily to identify any deceased animals. All deceased mice were examined for the presence of MI as well as pleural effusion and cardiac rupture, based on a diagnosis of the presence of a blood clot within the chest cavity in the postmortem examination.

2.4. Experimental protocol 2: 3-day post-MI study

Because a substantial portion of the MI animals died within 7 days after MI, in vivo LV function and myocardial histopathology were also evaluated in a separate group of additional $p53^{-/-}$ ($p53^{-/-}$ +MI), $p53^{+/-}$ ($p53^{+/-}$ +MI), and sibling wild-type mice ($p53^{+/+}$ +MI) at 3 days of surgery treated identically to experimental protocol 1. A sham operation without coronary artery ligation was also performed in both $p53^{+/+}$ ($p53^{+/+}$ +Sham) and $p53^{+/-}$ ($p53^{+/-}$ +Sham) mice. The numbers of $p53^{-/-}$ mice were less than those of $p53^{+/-}$ mice because of the limited number of $p53^{-/-}$ mice available for the detailed subsequent analysis. In fact, the previous study has shown that a significant proportion of female $p53^{-/-}$ mice die during embryogenesis or in the period between birth and weaning [15]. In addition, in $p53^{-/-}$ female embryos, the normal process of neural tube closure failed, leading to exencephaly and subsequent anencephaly. Another possible explanation for the lower availability of $p53^{-/-}$ mice is that p53 is involved in the normal process of spermatogenesis [16].

2.4.1. Echocardiographic and hemodynamic measurements

Echocardiographic studies were performed under light anesthesia with tribromoethanol/amylene hydrate (Avertin; 2.5% wt./vol., 8 μ L/g ip) and spontaneous respiration [14]. A

two-dimensional parasternal short-axis view of the LV was obtained at the level of the papillary muscles. In general, the best views were obtained with the transducer lightly applied to the mid upper left anterior chest wall. The transducer was then gently moved cephalad or caudad and angulated until desirable images were obtained. After confirming that the imaging was on axis (based on roundness of the LV cavity), two-dimensional targeted M-mode tracings were recorded at a paper speed of 50 mm/s. Next, a 1.4 Fr micromanometer-tipped catheter (Millar) was inserted into the right carotid artery and then was advanced into the left ventricle to measure the LV pressures. One subset of two investigators, who were not informed of the experimental groups, performed *in vivo* LV function studies. Our recent validation study has shown that the intraobserver and interobserver variabilities of our echocardiographic measurements for LV cavity dimensions and fractional shortening were small and measurements made in the same animals on separate days were highly reproducible [14].

2.4.2. Infarct size and wall thickness

Infarct size was determined by the methods described in rats [17] and also in mice [18,19]. The heart was excised and the right and left ventricles including the septum were dissected. The left ventricles were cut from apex to base into 3 transverse sections. Five- μ m sections were cut and stained with Masson's trichrome. Infarct length was measured along the endo- and epicardial surfaces from each of the LV sections, and the values from all specimens were summed. Total LV circumference was calculated as the sum of endo- and epicardial segment lengths from all LV sections. Infarct size (in percent) was calculated as total infarct circumference divided by total LV circumference. In our preliminary study, we confirmed excellent reliability of infarct size measurements, in which a morphometric methodology similar to that used in this study was employed. The intraobserver and interobserver variabilities between two measurements divided by the mean of the two measurements, expressed as a percentage, were less than 5%. Therefore, our technique could be considered to allow reliable assessment of infarct size in mice.

To further evaluate the effects of p53 on the risk area and infarct size, a separate group of animals including p53^{+/-}+MI ($n=5$) and p53^{+/+}+MI ($n=5$) was created. After 24 h, Evans blue dye (1%) was perfused into the aorta and coronary arteries with distribution throughout the LV wall proximal to the site of coronary artery ligation. The nonischemic area was stained blue. Hearts were excised and sliced into cross-sections below the ligature. These sections were weighed and then incubated with a 1% triphenyltetrazolium chloride (TTC) solution at 37 °C for 20 min. The infarct area (pale), the area at risk (not blue), and the total LV area from each section were measured, multiplied by the weight of the section, and then totaled from all sections [20].

To quantitate wall thinning, the thickness of the infarct wall was determined using the leading-edge method at the

thinnest point of transmural infarction. The noninfarct wall measurement was then acquired from the same slide at the point on the LV diametrically opposed to the point used for infarct thinning. The wall thinning was calculated by dividing the infarct wall thickness by the noninfarct wall thickness [21, 22].

2.4.3. Myocardial histopathology

From the mid-LV transverse sections, 5- μ m sections were cut and stained with hematoxylin and eosin and Masson's trichrome. To quantify myocardial infiltrates, nuclear density (nuclei per square millimeter) was determined. In each animal, 5 independent high-powered fields were analyzed. To further determine the number of macrophages, an immunohistochemical analysis using a specific antibody against mouse Mac-3 (BD Pharmingen) was performed.

The collagen volume fraction was determined by the quantitative morphometry of Masson's trichrome-stained mid-LV sections. Interstitial collagens were also stained with Sirius red.

2.4.4. MMP zymography

Zymographic MMP levels including MMP-2 and MMP-9 were determined in the infarcted LV using gelatin zymography [23].

2.4.5. Apoptosis

To detect apoptosis, LV tissue sections were stained with terminal deoxynucleotidyl transferase-mediated dUTP nick end-labeling (TUNEL) staining (TaKaRa). The number of TUNEL-positive nuclei was counted in the infarcted and border zone LV, and the data were normalized per 10⁵ total nuclei identified by hematoxylin-positive staining in the same sections. We further examined whether apoptosis is present by the more sensitive ligation-mediated PCR fragmentation assays (Maxim Biotech Inc.).

2.4.6. Akt protein

The Akt protein levels were analyzed in cardiac tissue homogenates by Western blot analysis with a polyclonal

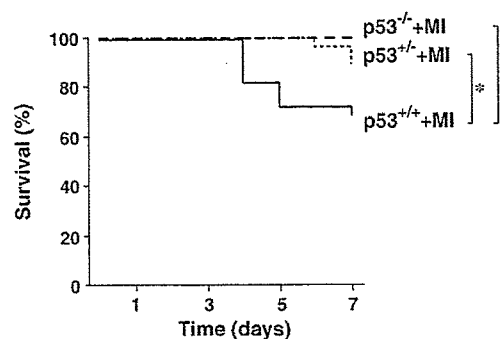


Fig. 2. Kaplan–Meier analysis of survival after MI in p53^{+/-}+MI ($n=29$), and p53^{+/-}+MI ($n=28$), and p53^{+/+}+MI ($n=20$) mice. There was no death after the sham operation in p53^{+/-} and p53^{-/-} mice (data not shown). * $P<0.05$ for difference from the p53^{+/-}+MI.

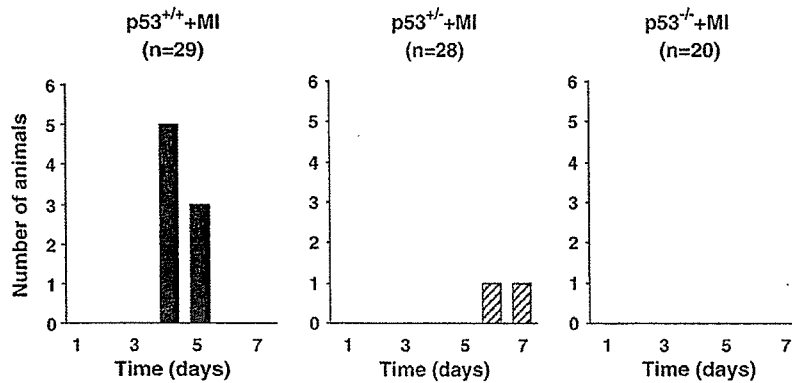


Fig. 3. The number of animals died of cardiac rupture in the p53^{+/+}+MI, p53^{+/-}+MI, and p53^{-/-}+MI mice.

antibody against phospho (Ser473)-Akt and Akt (Cell Signaling). In brief, the LV tissue was homogenized with the lysis buffer (25 mmol/L Tris, 150 mmol/L NaCl, 5 mmol/L EDTA, 1 mmol/L Na₃VO₄; pH 7.4). After centrifugation, equal amounts of protein (15 µg protein/lane), estimated by the Bradford method using a protein assay (Bio-Rad), were electrophoresed on a 12.5% SDS-polyacrylamide gel, and then electrophoretically transferred to a nitrocellulose membrane (Millipore). After blocking with 2.5% nonfat milk in TBS containing 0.1% Tween 20 at room temperature for 30 min, the membrane was incubated with the first antibody, and then with the peroxidase-linked second antibody (Santa Cruz). Chemiluminescence was detected with an ECL Western blot detection kit (Amersham Pharmacia) according to the manufacturer's recommendation.

2.5. Statistical analysis

All data are expressed as the means ± S.E.M. A survival analysis was performed by the Kaplan–Meier method, and between-group difference in survival was tested by the logrank test. Between-group comparisons of the means were performed by one-way ANOVA, followed by *t*-tests. The

Bonferroni's correction was done for multiple comparisons of the means.

3. Results

3.1. Experimental protocol 1: 7-day post-MI study

3.1.1. Survival and LV rupture

p53^{+/-}+MI and p53^{-/-}+MI mice had significantly better survival than p53^{+/+}+MI mice (Fig. 2). The number of the mice that died of LV rupture was significantly less in p53^{-/-}+MI and p53^{+/-}+MI than in p53^{+/+}+MI mice (Fig. 3). There were no deaths in the sham-operated groups. There were no significant differences in the survival rate among these 3 groups of survivor mice followed after 7 days up to 4 weeks.

3.2. Experimental protocol 2: 3-day post-MI study

3.2.1. Echocardiography and hemodynamics

The echocardiographic and hemodynamic data of the surviving mice at 3 days of MI are shown in Table 1. The LV diameters increased and fractional shortening decreased significantly in the p53^{+/+}+MI, p53^{+/-}+MI, and p53^{-/-}+MI

Table 1
Echocardiographic and hemodynamic data at 3 days after surgery

	p53 ^{+/+} +Sham	p53 ^{+/-} +Sham	p53 ^{+/+} +MI	p53 ^{-/-} +MI	p53 ^{-/-} +MI
Echocardiographic data					
<i>n</i>	7	7	13	12	7
Heart rate, bpm	491 ± 3	487 ± 5	492 ± 7	493 ± 5	484 ± 15
LV EDD, mm	3.7 ± 0.1	3.7 ± 0.1	4.6 ± 0.1**	4.7 ± 0.1**	4.7 ± 0.1**
LV ESD, mm	2.3 ± 0.0	2.3 ± 0.1	3.9 ± 0.1**	3.8 ± 0.1**	3.8 ± 0.1**
Fractional shortening, %	36.6 ± 0.4	37.7 ± 0.4	16.5 ± 1.0**	17.9 ± 0.7**	19.2 ± 1.0**
Hemodynamic data					
<i>n</i>	7	7	11	10	5
Heart rate, bpm	492 ± 14	491 ± 10	481 ± 15	490 ± 13	494 ± 6
Mean aortic pressure, mm Hg	79 ± 4	79 ± 2	77 ± 2	79 ± 2	74 ± 1
LV EDP, mm Hg	1.3 ± 0.4	1.3 ± 0.4	12.0 ± 1.9**	11.7 ± 2.9**	10.2 ± 2.8**
LV dP/dt _{max} , mm Hg/s	9055 ± 1133	8299 ± 332	5927 ± 409**	5710 ± 240**	6417 ± 466**

MI, myocardial infarction. LV, left ventricular. EDD, end-diastolic diameter. ESD, end-systolic diameter. EDP, end-diastolic pressure. bpm, beats per min. Values are means ± S.E.M. ***P* < 0.01 vs. p53^{+/-}+Sham.

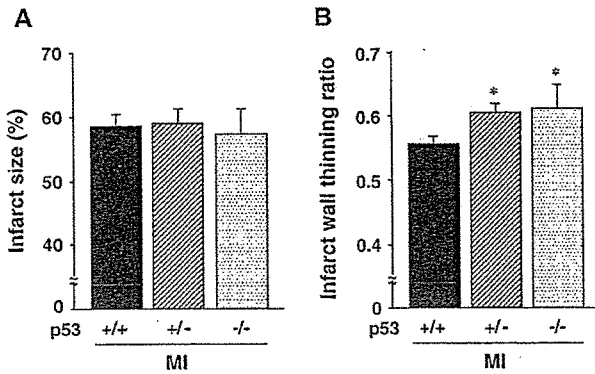


Fig. 4. Infarct size (A) and infarct wall thinning ratio (B) in $p53^{+/+}$ -MI, $p53^{-/-}$ -MI, and $p53^{-/-}$ -MI mice ($n=6$ each). Values are means \pm S.E.M. * $P<0.05$ for difference from the $p53^{+/+}$ -MI.

MI mice compared to sham operated mice. However, these changes were comparable among $p53^{+/+}$ -MI, $p53^{+/-}$ -MI, and $p53^{-/-}$ -MI.

There was no significant difference in the heart rate and mean aortic blood pressure among 5 groups of mice. The LV end-diastolic pressure (EDP) increased and LV dP/dt_{max} decreased in $p53^{+/+}$ -MI compared to sham, which was similarly observed in $p53^{+/-}$ -MI and $p53^{-/-}$ -MI.

3.2.2. Infarct size and wall thickness

The infarct size determined by the morphometric analysis at 3 days of MI was comparable among the $p53^{+/+}$ -MI, $p53^{+/-}$ -MI, and $p53^{-/-}$ -MI ($n=6$ each) mice (Fig. 4A). Moreover, percentages of LV at risk (risk area/LV; $60.4 \pm 5.2\%$ vs. $59.1 \pm 2.8\%$, $P=NS$) and the infarct size (infarct/risk area; $58.7 \pm 7.8\%$ vs. $61.4 \pm 2.5\%$, $P=NS$) measured by Evans blue and TTC staining at 24 h of MI were also comparable between $p53^{+/-}$ -MI and $p53^{+/+}$ -MI ($n=5$ each).

The thickness of the infarcted LV wall and that of the noninfarcted LV in $p53^{-/-}$ -MI were 0.43 ± 0.02 and 0.70 ± 0.03 mm, respectively, those in $p53^{+/-}$ -MI were 0.41 ± 0.02 and 0.67 ± 0.03 mm, respectively, and those in $p53^{+/+}$ -MI were 0.39 ± 0.01 and 0.70 ± 0.02 mm, respectively. Thus infarct wall thinning ratio, the thickness of the infarcted LV wall normalized to that of the noninfarcted LV, was significantly greater in $p53^{-/-}$ -MI or $p53^{+/-}$ -MI than in $p53^{+/+}$ -MI (Fig. 4B).

3.2.3. Myocardial histopathology

MI mice had more infiltrating interstitial cells in the border zone and infarcted myocardium than sham-operated mice. However, the extent of infiltration was comparable among $p53^{+/+}$ -MI, $p53^{+/-}$ -MI, and $p53^{-/-}$ -MI (Fig. 5A). Moreover, the infiltration of macrophages was similar between groups (Fig. 5B).

Interstitial fibrosis, measured as collagen volume fraction, in the infarcted as well as border zone LV was also comparable among $p53^{+/+}$ -MI, $p53^{+/-}$ -MI, and $p53^{-/-}$ -MI (Fig. 6A).

3.2.4. MMPs

The zymographic MMP-2 and MMP-9 levels significantly increased in the infarcted LV from MI groups, however, no difference in this regard was seen between $p53^{+/+}$ -MI and $p53^{+/-}$ -MI mice (Fig. 6B).

3.2.5. Myocardial apoptosis

There were rare TUNEL-positive nuclei in sham-operated mice. The number of TUNEL-positive cells was increased in $p53^{+/+}$ -MI, which was significantly prevented in $p53^{+/-}$ -MI and $p53^{-/-}$ -MI (Fig. 7A). In addition, DNA ladder appeared faint in the infarcted LV from $p53^{+/-}$ -MI compared to that from $p53^{+/+}$ -MI (Fig. 7B).

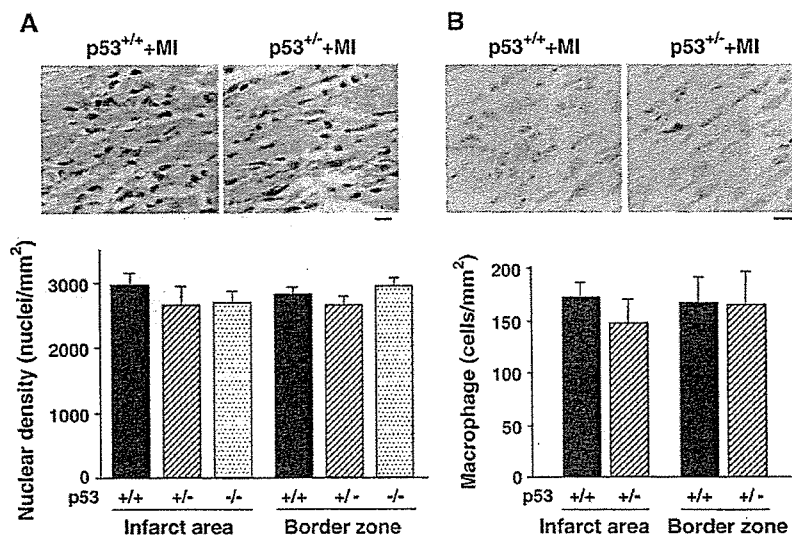


Fig. 5. Representative photomicrographs of LV sections and summary data for nuclear density of infiltrating cells stained with hematoxylin and eosin (A) and macrophages (B) at the infarct area and border zone. Scale bar, 10 μ m. Values are means \pm S.E.M. ($n=6$ each).

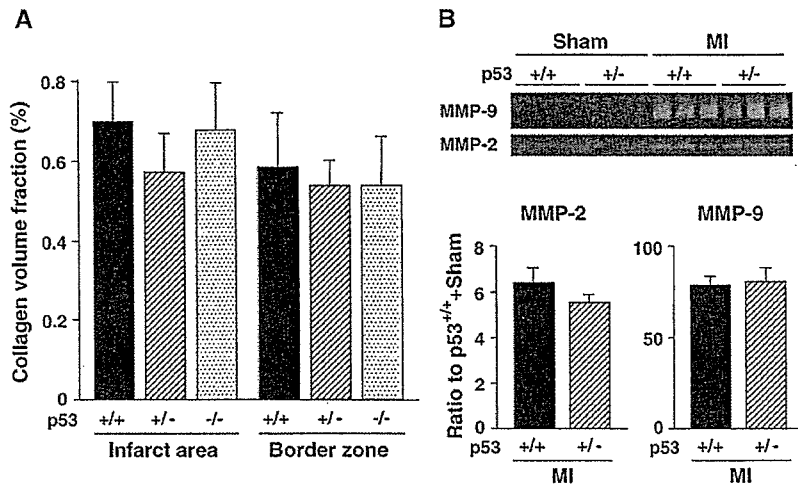


Fig. 6. (A) Summary data of collagen volume fraction at the infarcted area and border zone of LV tissue sections ($n=6$ for each). (B) Representative LV zymographic MMP-2 and MMP-9 levels and summary data at 3 days of MI ($n=6$ for each).

3.2.6. Akt protein

Either Akt protein (total) or phospho-Akt levels did not differ between 4 groups of p53^{+/+}+Sham, p53^{+/-}+Sham, p53^{+/+}+MI, and p53^{+/-}+MI mice (Fig. 8).

4. Discussion

The major new finding of the present study is the significant improvement in the survival of MI mice by the targeted deletion of p53 gene, which was mainly attributable to the inhibition of early LV rupture. After MI, p53-dependent apoptosis might contribute to the thinning of the infarct wall and eventual LV rupture. Our observations thus

suggest that an anti-p53 strategy may be of therapeutic benefit against the evolution of cardiac rupture after MI.

Cardiac rupture is the most drastic and severe complication of acute MI. Following MI, a reparative process, infarct healing, is immediately initiated, including inflammatory cell infiltration, activation of MMPs, extracellular matrix remodeling and scar formation. Thinning of the infarcted wall and dilatation of LV cavity, which occur during the acute phase of MI, are termed as “infarct expansion” [1]. The delay or impairment of this process may jeopardize infarct healing, aggravate extracellular matrix remodeling, and cause cardiac rupture. Previous studies demonstrated that p53 was increased [8] and apoptosis of cardiac myocytes were detected in the infarcted regions during the

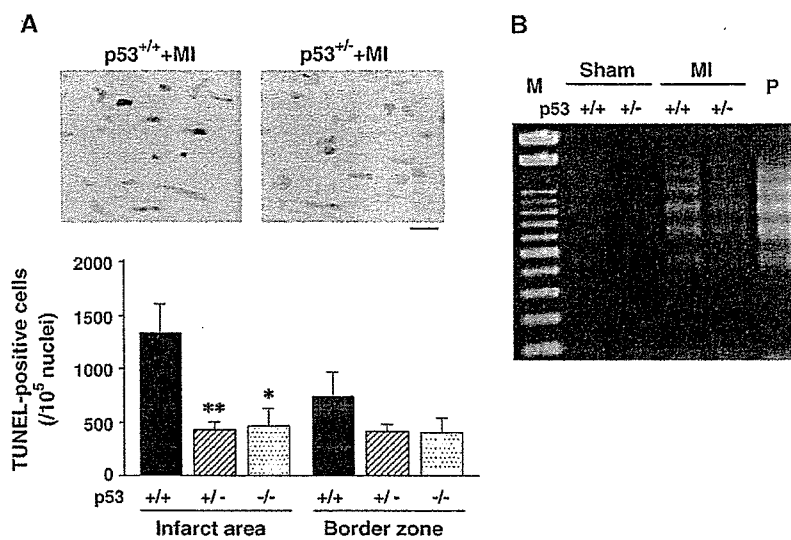


Fig. 7. (A) Representative photomicrographs of LV sections and summary data for the number of TUNEL-positive cells in the infarcted area and border zone of LV ($n=6$ each). Scale bar, 10 μ m. Values are means \pm S.E.M. * $P < 0.05$, ** $P < 0.01$ for difference from the p53^{+/+}+MI values. (B) DNA ladder indicative of apoptosis in the genomic DNA from the LV. M, marker. P, positive control.

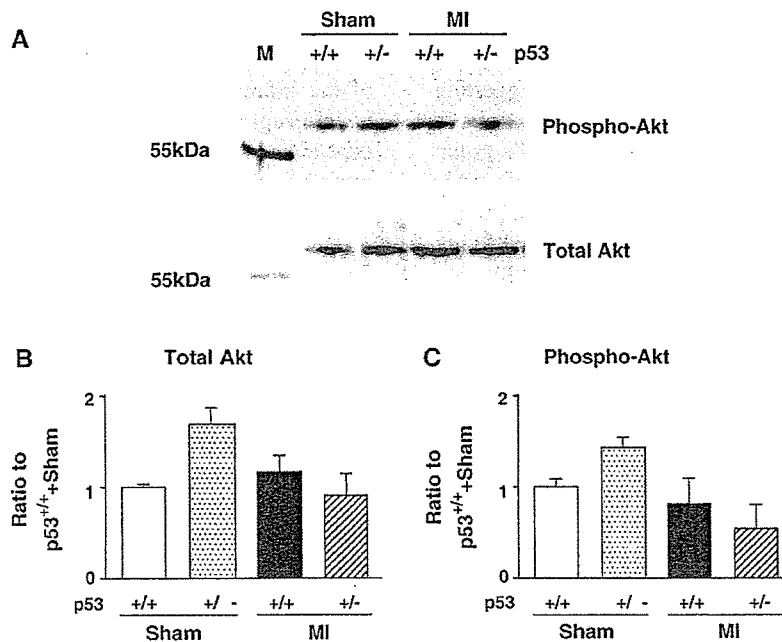


Fig. 8. (A) Representative Western blot analysis of Akt (total) and phospho-Akt protein levels in LV tissue obtained from 4 groups of $p53^{+/+}$ + Sham, $p53^{+/-}$ + Sham, $p53^{+/+}$ + MI, and $p53^{+/-}$ + MI mice. Summary data for total Akt (B) and phospho-Akt (C) protein levels in $p53^{+/+}$ + Sham, $p53^{+/-}$ + Sham, $p53^{+/+}$ + MI, and $p53^{+/-}$ + MI mice ($n = 3$ for each). M, marker.

early days after MI [9,10]. Therefore, p53-dependent apoptosis at the infarcted myocardium may contribute to cardiac rupture. However, no previous studies have provided direct evidence supporting this notion. The present study has demonstrated that p53 is indeed involved in cardiac rupture after MI (Fig. 3) via mediating apoptosis (Fig. 7) and wall thinning at the infarct area (Fig. 4B).

The beneficial effects of p53 deletion were not due to its MI size-sparing effects because the infarct size was comparable between the $p53^{+/+}$ and $p53^{+/-}$ mice (Fig. 4A). Further, its effects might not be attributable to those on hemodynamics because the blood pressure and heart rate showed no alterations (Table 1). In addition, inflammatory cell infiltration and inadequate fibrosis have been postulated to cause myocyte separation in the infarct area, which may lead to eventual cardiac rupture [4]. However, the present study could not find any alterations in the infiltration of inflammatory cells or collagen deposition between $p53^{+/+}$ and $p53^{+/-}$ mice after MI (Figs. 5 and 6A). Further, even though recent studies have demonstrated that the inhibition of MMPs can prevent cardiac rupture [4,5], targeted deletion of p53 gene did not affect the increase in MMP-2 or MMP-9 activities in the post-MI hearts in the present study (Fig. 6B). These lines of evidence indicate that the inhibition of cardiac rupture in $p53^{+/-}$ mice was not due to the altered reparative process of extracellular matrix or the infiltration of inflammatory cells and further confirm the significance of attenuated apoptosis and infarct wall thinning in the prevention of cardiac rupture.

Previous experimental [9] and human [10] studies have detected TUNEL-positive cells in the post-MI hearts. Even

though they implicated apoptosis in the pathogenesis of late LV remodeling after MI [19], it may also contribute to the early phase structural alterations known to occur within the infarct area, which is characterized by a significant net loss of cardiac myocytes as well as myocyte slippage and elongation [24]. However, the significance of myocardial apoptosis in this phase of MI has been mostly speculative. Thus the present study clearly demonstrated for the first time that p53-dependent apoptosis is involved not only in late remodeling after MI [19] but also in early cardiac rupture.

The present study was in contrast to the previous study by Bialik et al., in which myocyte apoptosis was not altered after MI in the hearts of mice nullizygous for p53 [25]. It is difficult, however, to find identical experimental conditions between their study and the present study by that would be necessary for a direct comparison; the age of the animals (6–8 weeks in the study by Bialik vs. 10–14 weeks in this study) and the time at which apoptosis was assessed (10 and 48 h vs. 3 days). In addition, the infarct size was comparable between $p53^{-/-}$ and $p53^{+/-}$ in the present study although it was not clearly mentioned in the study by Bialik. Although the present study demonstrated the survival benefit in p53 deletion, no survival data were provided in their study.

p53 is known to be dynamically regulated via Akt, a serine/threonine kinase, that promotes cell survival [26]. Specifically, proapoptotic stimulation leads to p53-dependent destruction of Akt whereas Akt activation leads to inhibition of p53. The state of this signaling network determines the fate of the cell to survive or to enter apoptosis or hypertrophy. However, either Akt protein

(total) or phospho-Akt levels did not differ between 4 groups of p53^{+/+}+Sham, p53^{+/-}+Sham, p53^{+/+}+MI, and p53^{+/-}+MI mice in the present study (Fig. 8), suggesting that Akt might not play a major role in myocyte apoptosis in this model. Moreover, a recent study by Dr. Field's group has demonstrated that p193 and p53 exert a cell cycle regulatory role in the adult heart [27]. In their studies, target expression of the p193 and/or the p53 dominant-interfering mutants increased cardiac myocyte DNA synthesis after MI in mice, suggesting that cardiac cell cycle reentry is regulated by these proapoptotic proteins. Therefore, we could not exclude the possibility that p193 might also be involved in post-MI remodeling.

Even though the previous studies reported a difference in the phenotype between p53^{-/-} and p53^{+/-} mice [15,16], the echocardiographic data (Table 1), hemodynamic data (Table 1), infarct size (Fig. 4), infarct wall thinning ratio (Fig. 4), nuclear density (Fig. 5), collagen volume fraction by myocardial histopathology (Fig. 6), and the number of TUNEL-positive cells (Fig. 7) were comparable between these 2 groups of mice in the present study. Based on these results, there might be a threshold in the effects of p53 gene expression on cardiac pathophysiology after MI.

There are several limitations to be acknowledged in this study. First, although p53 is activated in the post-MI hearts [8], the mechanisms responsible for this activation are not determined in the present study. One important aspect of ischemia is prolonged hypoxia, which has been shown to increase p53 expression and result in apoptosis in cultured cardiac myocytes [6]. Furthermore, oxidative stress, which is also increased in post-MI hearts, is a powerful inducer of apoptosis [28]. However, further studies are needed to clarify the mechanisms for the modulation of p53 after MI. Second, even though the previous study demonstrated that p53 expression was increased in post-MI rat hearts [8], the present study did not determine whether endogenous p53 expression was altered in post-MI mouse hearts. Third, p53-dependent apoptotic pathways may not be a sole mechanism for cardiac rupture after MI. Cardiac repair after MI is a highly complex process, involving diverse inflammatory and growth factor signaling pathways, and extracellular matrix remodeling. Thus the mechanisms other than p53 may be also involved in this deleterious complication. Fourth, echocardiographic assessment of LV function in mice is known to be difficult. However, intra- and interobserver variabilities of our echocardiographic measurements for LV cavity dimensions and fractional shortening were small and measurements were highly reproducible [14]. Therefore, our technique was capable of noninvasively assessing the LV structure and function in mice with a large MI.

Cardiac rupture usually occurs unexpectedly and is often fatal, thereby resulting in one of the major causes of in-hospital death in patients with acute MI. It is difficult to predict its occurrence by the previously reported clinical risk factors such as aging, hypertension, and delayed thrombolysis [29]. We found that target deletion of p53 had a

significantly reduced cardiac rupture rate after MI. This was accompanied by a reduction of apoptosis and wall thinning of the infarcted myocardium. Our results may provide a novel insight regarding the pathophysiological role of p53-dependent apoptosis in cardiac rupture and thus help to establish an effective therapeutic strategy.

Acknowledgments

This study was supported in part by grants from the Ministry of Education, Science and Culture (Nos. 120670676, 14370230, 17390223). A part of this study was conducted in Kyushu University Station for Collaborative Research I and II.

References

- [1] Pfeffer JM, Pfeffer MA, Fletcher PJ, Braunwald E. Progressive ventricular remodeling in rat with myocardial infarction. *Am J Physiol* 1991;260:H1406–14.
- [2] Anzai T, Yoshikawa T, Shiraki H, Asakura Y, Akaishi M, Mitamura H, et al. C-reactive protein as a predictor of infarct expansion and cardiac rupture after a first Q-wave acute myocardial infarction. *Circulation* 1997;96:778–84.
- [3] Przyklenk K, Connolly CM, McLaughlin RJ, Kloner RA, Apstein CS. Effect of myocyte necrosis on strength, strain, and stiffness of isolated myocardial strips. *Am Heart J* 1987;114:1349–59.
- [4] Heymans S, Lutun A, Nuyens D, Theilmeier G, Creemers E, Moons L, et al. Inhibition of plasminogen activators or matrix metalloproteinases prevents cardiac rupture but impairs therapeutic angiogenesis and causes cardiac failure. *Nat Med* 1999;5:1135–42.
- [5] Matsumura S, Iwanaga S, Mochizuki S, Okamoto H, Ogawa S, Okada Y. Targeted deletion or pharmacological inhibition of MMP-2 prevents cardiac rupture after myocardial infarction in mice. *J Clin Invest* 2005;115:599–609.
- [6] Long X, Boluyt MO, Hipolito ML, Lundberg MS, Zheng JS, O'Neill L, et al. p53 and the hypoxia-induced apoptosis of cultured neonatal rat cardiac myocytes. *J Clin Invest* 1997;99:2635–43.
- [7] Polyak K, Xia Y, Zweier JL, Kinzler KW, Vogelstein B. A model for p53-induced apoptosis. *Nature* 1997;389:300–5.
- [8] Oskarsson HJ, Coppey L, Weiss RM, Li WG. Antioxidants attenuate myocyte apoptosis in the remote non-infarcted myocardium following large myocardial infarction. *Cardiovasc Res* 2000;45:679–87.
- [9] Kajstura J, Cheng W, Reiss K, Clark WA, Sonnenblick EH, Krajewski S, et al. Apoptotic and necrotic myocyte cell deaths are independent contributing variables of infarct size in rats. *Lab Invest* 1996;74:86–107.
- [10] Saraste A, Pulkki K, Kallajoki M, Henriksen K, Parvinen M, Voipio-Pulkki LM. Apoptosis in human acute myocardial infarction. *Circulation* 1997;95:320–3.
- [11] Mayr U, Mayr M, Li C, Wernig F, Dietrich H, Hu Y, et al. Loss of p53 accelerates neointimal lesions of vein bypass grafts in mice. *Circ Res* 2002;90:197–204.
- [12] Donehower LA, Harvey M, Slagle BL, McArthur MJ, Montgomery CA, Butel JS, et al. Mice deficient for p53 are developmentally normal but susceptible to spontaneous tumours. *Nature* 1992;356:215–21.
- [13] Ducharme A, Frantz S, Aikawa M, Rabkin E, Lindsey M, Rohde LE, et al. Targeted deletion of matrix metalloproteinase-9 attenuates left ventricular enlargement and collagen accumulation after experimental myocardial infarction. *J Clin Invest* 2000;106:55–62.
- [14] Shiomi T, Tsutsui H, Hayashidani S, Suematsu N, Ikeuchi M, Wen J, et al. Pioglitazone, a peroxisome proliferator-activated receptor-

- gamma agonist, attenuates left ventricular remodeling and failure after experimental myocardial infarction. *Circulation* 2002;106:3126–32.
- [15] Armstrong JF, Kaufman MH, Harrison DJ, Clarke AR. High-frequency developmental abnormalities in p53-deficient mice. *Curr Biol* 1995;5:931–6.
- [16] Rotter V, Schwartz D, Almon E, Goldfinger N, Kapon A, Meshorer A, et al. Mice with reduced levels of p53 protein exhibit the testicular giant-cell degenerative syndrome. *Proc Natl Acad Sci U S A* 1993;90:9075–9.
- [17] Pfeffer MA, Pfeffer JM, Fishbein MC, Fletcher PJ, Spadaro J, Kloner RA, et al. Myocardial infarct size and ventricular function in rats. *Circ Res* 1979;44:503–12.
- [18] Patten RD, Aronovitz MJ, Deras-Mejia L, Pandian NG, Hanak GG, Smith JJ, et al. Ventricular remodeling in a mouse model of myocardial infarction. *Am J Physiol* 1998;274:H1812–20.
- [19] Sam F, Sawyer DB, Chang DL, Eberli FR, Ngoy S, Jain M, et al. Progressive left ventricular remodeling and apoptosis late after myocardial infarction in mouse heart. *Am J Physiol Heart Circ Physiol* 2000;279:H422–8.
- [20] Ikeuchi M, Tsutsui H, Shiomi T, Matsusaka H, Matsushima S, Wen J, et al. Inhibition of TGF-beta signaling exacerbates early cardiac dysfunction but prevents late remodeling after infarction. *Cardiovasc Res* 2004;64:526–35.
- [21] Delyani JA, Robinson EL, Rudolph AE. Effect of a selective aldosterone receptor antagonist in myocardial infarction. *Am J Physiol Heart Circ Physiol* 2001;281:H647–54.
- [22] Lindsey ML, Gannon J, Aikawa M, Schoen FJ, Rabkin E, Lopresti-Morrow L, et al. Selective matrix metalloproteinase inhibition reduces left ventricular remodeling but does not inhibit angiogenesis after myocardial infarction. *Circulation* 2002;105:753–8.
- [23] Hayashidani S, Tsutsui H, Ikeuchi M, Shiomi T, Matsusaka H, Kubota T, et al. Targeted deletion of MMP-2 attenuates early LV rupture and late remodeling after experimental myocardial infarction. *Am J Physiol Heart Circ Physiol* 2003;285:H1229–35.
- [24] Li Q, Li B, Wang X, Leri A, Jana KP, Liu Y, et al. Overexpression of insulin-like growth factor-1 in mice protects from myocyte death after infarction, attenuating ventricular dilation, wall stress, and cardiac hypertrophy. *J Clin Invest* 1997;100:1991–9.
- [25] Bialik S, Geenen DL, Sasson IE, Cheng R, Horner JW, Evans SM, et al. Myocyte apoptosis during acute myocardial infarction in the mouse localizes to hypoxic regions but occurs independently of p53. *J Clin Invest* 1997;100:1363–72.
- [26] Sussman MA, Anversa P. Myocardial aging and senescence: where have the stem cells gone? *Annu Rev Physiol* 2004;66:29–48.
- [27] Nakajima H, Nakajima HO, Tsai SC, Field LJ. Expression of mutant p193 and p53 permits cardiomyocyte cell cycle reentry after myocardial infarction in transgenic mice. *Circ Res* 2004;94:1606–14.
- [28] von Harsdorf R, Li PF, Dietz R. Signaling pathways in reactive oxygen species-induced cardiomyocyte apoptosis. *Circulation* 1999;99:2934–41.
- [29] Maggioni AP, Maseri A, Fresco C, Franzosi MG, Mauri F, Santoro E, et al. Age-related increase in mortality among patients with first myocardial infarctions treated with thrombolysis. The Investigators of the Gruppo Italiano per lo Studio della Sopravvivenza nell'Infarto Miocardico (GISSI-2). *N Engl J Med* 1993;329:1442–8.

Targeted Deletion of Matrix Metalloproteinase 2 Ameliorates Myocardial Remodeling in Mice With Chronic Pressure Overload

Hidehori Matsusaka, Tomomi Ide, Shouji Matsushima, Masaki Ikeuchi, Toru Kubota, Kenji Sunagawa, Shintaro Kinugawa, Hiroyuki Tsutsui

Abstract—Matrix metalloproteinases (MMPs) play an important role in the extracellular matrix remodeling. Experimental and clinical studies have demonstrated that MMP 2 and 9 are upregulated in the dilated failing hearts and involved in the development and progression of myocardial remodeling. However, little is known about the role of MMPs in mediating adverse myocardial remodeling in response to chronic pressure overload (PO). We, thus, hypothesized that selective disruption of the MMP 2 gene could ameliorate PO-induced cardiac hypertrophy and dysfunction in mice. PO hypertrophy was induced by transverse aortic constriction (TAC) in male MMP 2 knockout (KO) mice (n=10) and sibling wild-type (WT) mice (n=9). At 6 weeks, myocardial MMP 2 zymographic activity was 2.4-fold increased in WT+TAC, and this increase was not observed in KO+TAC, with no significant alterations in other MMPs (MMP 1, 3, 8, and 9) or tissue inhibitors of MMPs (1, 2, 3, and 4). TAC resulted in a significant increase in left ventricular (LV) weight and LV end-diastolic pressure (EDP) with preserved systolic function. KO+TAC mice exerted significantly lower LV weight/body weight (4.2 ± 0.2 versus 5.0 ± 0.2 mg/g; $P<0.01$), lung weight/body weight (4.9 ± 0.2 versus 6.2 ± 0.4 mg/g; $P<0.01$), and LV end-diastolic pressure (4 ± 1 versus 10 ± 2 mm Hg; $P<0.05$) than WT+TAC mice despite comparable aortic pressure. KO+TAC mice had less myocyte hypertrophy (cross-sectional area; 322 ± 14 versus 392 ± 14 μm^2 ; $P<0.01$) and interstitial fibrosis (collagen volume fraction; 3.3 ± 0.5 versus $8.2\pm 1.0\%$; $P<0.01$) than WT+TAC mice. MMP 2 plays an important role in PO-induced LV hypertrophy and dysfunction. The inhibition of MMP 2 activation may, therefore, be a useful therapeutic strategy to manage hypertensive heart disease. (*Hypertension*. 2006;47:711-717.)

Key Words: hypertrophy ■ heart failure ■ fibrosis ■ extracellular matrix ■ hypertension, experimental ■ myocardium

Left ventricular (LV) hypertrophy is an adaptive process that compensates for pressure overload (PO) caused by hypertension or valvular heart disease, such as aortic stenosis. This remodeling process consists of hypertrophic changes of cardiac myocytes and abnormalities of the extracellular matrix (ECM) network, which are both responsible for changes in systolic and diastolic function.¹

The dynamic synthesis and breakdown of ECM proteins play an important role in adverse myocardial remodeling. In particular, the increased expression and activation of the matrix metalloproteinases (MMPs) have been shown in various forms of heart failure and implicated in the process of myocardial remodeling that is characteristic of developing heart failure.² Despite a number of studies implicating MMPs in cardiac pathophysiology, little is known about the role of MMP in the development of myocardial remodeling in response to chronic PO. MMP 2 and 9 expression has been

shown to be enhanced in pressure-overloaded cardiac hypertrophy in spontaneously hypertensive rats³ and in Dahl salt-sensitive hypertensive rats.⁴ Similar upregulation of MMPs has been also observed in human pressure-overloaded hearts because of aortic stenosis.⁵ Recently, Heymans et al⁶ have demonstrated that MMP 9 is involved in cardiac remodeling associated with hypertension. However, MMP-9 is mainly expressed in such infiltrating inflammatory cells as neutrophils and macrophages.⁷ Conversely, MMP 2 is ubiquitously distributed in cardiac myocytes and fibroblasts.⁸ Therefore, MMP 2 may also play an important role in the development and progression of myocardial remodeling in response to PO. However, no previous studies have yet determined the pathophysiological significance of MMP 2 in this disease state.

In the present study, we evaluated the effects of a targeted deletion of the MMP 2 gene on both LV structural and

Received November 28, 2005; first decision December 13, 2005; revision accepted January 3, 2006.

From the Department of Cardiovascular Medicine (H.M., T.I., S.M., M.I., T.K., K.S.), Graduate School of Medical Sciences, Kyushu University, Fukuoka; and Department of Cardiovascular Medicine (S.K., H.T.), Hokkaido University Graduate School of Medicine, Sapporo, Japan.

Correspondence to Hiroyuki Tsutsui, Dept of Cardiovascular Medicine, Hokkaido University Graduate School of Medicine, Kita-15, Nishi-7, Kita-ku, Sapporo 060-8638, Japan. E-mail htsutsui@med.hokudai.ac.jp

© 2006 American Heart Association, Inc.

Hypertension is available at <http://www.hypertensionaha.org>

DOI: 10.1161/01.HYP.0000208840.30778.00

functional alterations during pressure-overloaded cardiac hypertrophy. To ensure selective and long-term complete inhibition of MMP 2, we used MMP 2 knockout (KO) mice.^{9–11} The most effective way to evaluate the contribution of the specific MMP and obtain the direct evidence for a role of MMP is through gene manipulation instead of MMP inhibitor.

Methods

Experimental Animals

The study was approved by our Institutional Animal Research Committee and conformed to the animal care guidelines of the American Physiological Society. We used the progeny of homozygous breeding pairs of C57BL/6J mice with targeted disruption of MMP 2 ranging in age from 11 to 14 weeks old.¹⁰ The mutation heterozygous mice were obtained by crossing the chimeras to C57BL/6J mice. Heterozygotes were backcrossed to C57BL/6J 1 to 5 times and then crossed to obtain the mutation homozygous mice. The original breeding pairs used to develop the mice for this study were obtained from Dr Shigeyoshi Itohara (Laboratory for Behavioral Genetics, RIKEN, Tsukuba, Japan).

Transverse Aortic Constriction

Transverse aortic constriction (TAC) was performed in male MMP 2 KO and sibling wild-type (WT) mice as described previously.¹² Briefly, after anesthetizing with tribromoethanol/amyline hydrate (Avertin; 2.5% weight/volume, 8 μ L/g IP), mice were intubated and ventilated, and a thoracotomy was performed via the second intercostal space at the left upper sternal border. The transverse aortic arch was ligated between the innominate and left common carotid arteries with an overlying 28-gauge needle, which, after removal of the needle, left a reproducible discrete region of stenosis. Sham-operated mice underwent a similar procedure without ligation of the aorta.

Tail clips and a PCR protocol to confirm the genotype were performed by a group of investigators. Next, TAC was induced in these mice by another subset of investigators, who were not informed of the genotyping results. This assignment procedure was performed using numeric codes to identify the animals.

MMPs and Tissue Inhibitors of MMPs

First, the myocardial MMP levels, including MMP 2 and MMP 9, were determined in the left ventricle (LV) using gelatin zymography as described previously.¹³ The LV myocardial samples were homogenized (\approx 30-s bursts) in 1 mL of an ice-cold extraction buffer containing cacodylic acid (10 mmol/L), NaCl (0.15 mol/L), ZnCl₂ (20 mmol/L), Na₂S (1.5 mmol/L), and 0.01% Triton X-100 (pH 5.0). The homogenate was then centrifuged (4°C, 10 minutes, 10 000g) and the supernatant decanted and saved on ice. The pH levels of the samples were adjusted to 7.5 using Tris (1 mol/L). The final protein concentration of the myocardial extracts was determined using a standardized colorimetric assay. The extracted samples were then aliquoted and stored at -80°C until the time of assay. The myocardial extracts were then directly loaded onto electrophoretic gels (SDS-PAGE) containing 1 mg/mL of gelatin under nonreducing conditions. The myocardial extracts at a final protein content of 5 μ g were loaded onto the gels using a 3:1 sample buffer (10% SDS, 4% sucrose, 0.25 mol/L Tris-Cl, and 0.1% bromophenol blue \leq pH 6.8]). The gels were run at 15 mA/gel through the stacking phase (4%) and at 20 mA/gel for the separating phase (10%), whereas the running buffer temperature was maintained at 4°C. After SDS-PAGE, the gels were washed twice in 2.5% Triton X-100 for 30 minutes each, rinsed in water, and incubated for 24 hours in a substrate buffer at 37°C (50 mmol/L Tris-HCl, 5 mmol/L, CaCl₂, and 0.02% Na₂S [pH 7.5]). After incubation, the gels were stained with Coomassie brilliant blue R-250. The zymograms were digitized, and the size-fractionated bands, which indicated the MMP proteolytic levels,

were measured by the integrated optical density in a rectangular region of interest.

Next, the mRNA levels of myocardial MMPs including MMP 1, 2, 3, 8, and 9 as well as tissue inhibitors of MMPs (TIMPs) including TIMP 1, 2, 3, and 4 were determined by multiprobe ribonuclease protection assay (RiboQuant, PharMingen). Each value was normalized to that of glyceraldehydes-3-phosphate-dehydrogenase in each template set as an internal control, followed by calculation as a ratio to WT+Sham. The amount of tissue was limited in mice and, thus, tissue needed to be divided so that all of the biochemical analyses could be performed.

Echocardiographic and Hemodynamic Measurements

Echocardiographic studies were performed under light anesthesia with tribromoethanol/amyline hydrate (Avertin; 2.5% weight/volume, 8 μ L/g IP) and spontaneous respiration as described previously.¹⁴ A 2D parasternal short-axis view of the LV was obtained at the level of the papillary muscles. In general, the best views were obtained with the transducer lightly applied to the mid-upper left anterior chest wall. The transducer was then gently moved cephalad or caudad and angulated until desirable images were obtained. After confirming that the imaging was on axis (based on roundness of the LV cavity), 2D targeted M-mode tracings were recorded at a paper speed of 50 mm/s. Two consecutive heartbeats of each frame were analyzed to measure the wall thickness and end-diastolic (EDD) and end-systolic (ESD) internal dimensions of the LV. LV fractional shortening (FS) was calculated as LV EDD minus LV ESD normalized for LV EDD and was taken as an index of LV systolic performance. Echocardiographic LV mass was calculated according to the standard cube formula as described previously.¹⁵ Our previous validation study has shown that the intraobserver and interobserver variabilities of our echocardiographic measurements for LV cavity dimensions and FS were small, and measurements made in the same animals on separate days were highly reproducible.¹⁴ Next, a 1.4-Fr micromanometer-tipped catheter (Millar) was inserted into the right carotid artery and then was advanced into the LV to measure the LV pressures. Arterial blood pressure and heart rate were also measured with the use of a noninvasive tail-cuff system (BP-98A, Softron).¹⁶

Organ Weight and Histopathology

After in vivo echocardiographic and hemodynamic studies, the heart and lung were excised, and their weights were determined. The heart was dissected into the right and left ventricles, including the septum. From the mid-LV transverse sections, 5- μ m sections were cut and stained with hematoxylin/eosin and Masson's trichrome to determine the myocyte cross-sectional area and collagen volume fraction. To measure the myocyte cross-sectional area, each section was photographed using a microscope and magnified (final magnification: \times 750). Connective tissue and muscle areas were identified, and the profile margin of 30 to 40 myocytes cut into cross-sections was manually traced and digitized. The digitized profiles were transferred to a personal computer that calculated the area. Three to 4 fields were randomly selected from 2 to 3 coronal sections of each heart. Thus, \approx 100 to 200 myocytes were measured for each animal, and the mean myocyte cross-sectional area was calculated.¹⁷ Collagen volume fraction was measured at \approx 5 to 7 fields for each heart.¹⁸ Within each field, segments representing connective tissue and myocyte were identified and manually traced by using a digitizing pad with a computer to calculate the traced area. Collagen volume fraction was then calculated for the heart as the sum of all of the connective tissue areas divided by the sum of all of the connective tissue and muscle areas in all fields. Collagen surrounding intramyocardial coronary arteries was excluded from the analysis.

Statistical Analysis

All of the data are expressed as the mean \pm SEM. Between-group comparisons of the means were performed by 1-way ANOVA, followed by *t* tests. The Bonferroni's correction was done for multiple comparisons of the means.

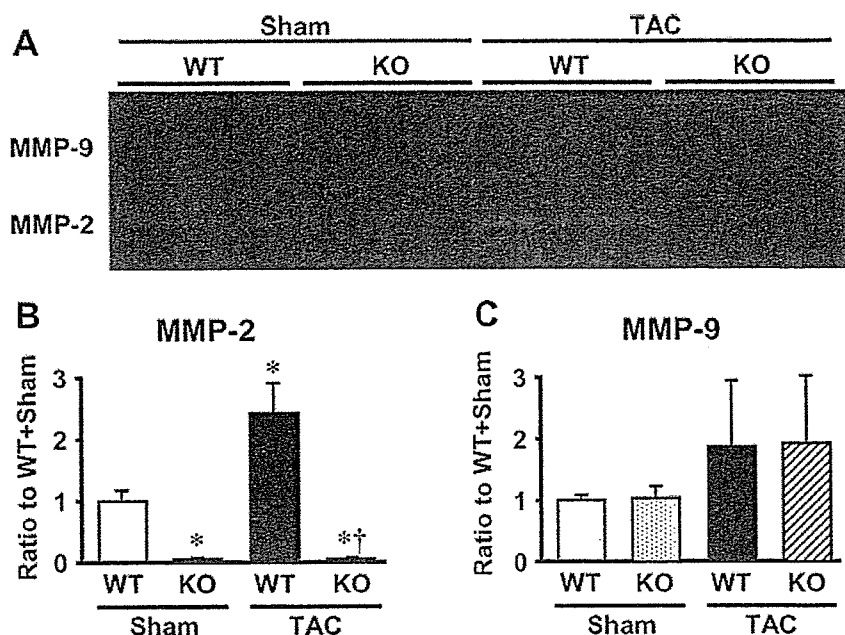


Figure 1. (A) Representative gelatin zymography of the LV from 4 groups of WT+Sham, KO+Sham, WT+TAC, and KO+TAC mice. (B and C) Densitometric analysis of MMP-2 (B) and MMP-9 (C) zymographic activity (n=3 each). Data are expressed as the ratio to WT+Sham values run concurrently on the same gel. Values are mean±SEM. *P<0.05 vs WT+Sham; †P<0.01 vs WT+TAC.

Results

MMPs and TIMPs

At 6 weeks of TAC, the zymographic MMP 2 levels increased by 2.4-fold compared with WT+Sham mice (Figure 1). As expected, MMP 2 activity was not detected in KO+Sham and KO+TAC mice. Importantly, the MMP 9 zymographic levels did not differ between WT+TAC and KO+TAC.

Again, the MMP 2 mRNA levels significantly increased in the WT+TAC compared with WT+Sham (Figure 2). This increase was not observed in KO+TAC. These results were consistent with those observed in gelatin zymography (Figure 1). Other MMPs, including MMP 1, 3, 8, and 9, were not altered in these mice (Figure 2). The changes of TIMPs (TIMP 1, 2, 3, and 4) were also comparable between WT+TAC and KO+TAC.

Echocardiography

The presence or absence of MMP 2 gene did not affect baseline heart rate or echocardiographic parameters in Sham mice (Table 1). TAC significantly increased LV wall thickness (Table 1) and echocardiographic LV mass (Figure 3) without affecting LV diameters or FS in WT+TAC. These LV hypertrophic changes in WT+TAC were significantly ameliorated in KO+TAC.

Hemodynamics

LV systolic pressure was markedly elevated by TAC (Table 2). However, there was no significant difference in LV systolic pressure between WT+TAC and KO+TAC mice. LV EDP increased significantly in WT+TAC mice, and this increase was significantly attenuated in KO+TAC mice.

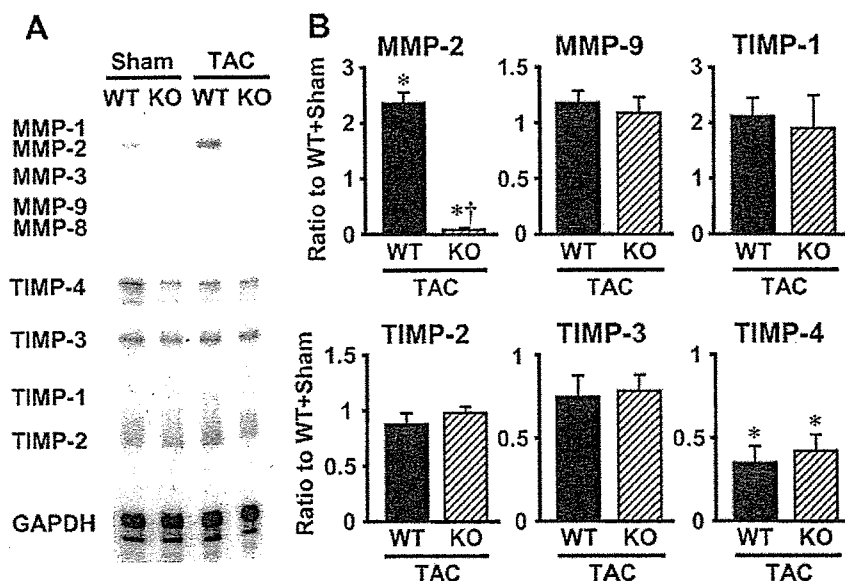


Figure 2. (A) Representative image of myocardial gene expression of MMPs and TIMPs. (B) Densitometric analysis of MMP and TIMP gene expression from WT+TAC (n=5) and KO+TAC (n=4). Each value was normalized to that of glyceraldehydes-3-phosphate-dehydrogenase in each template set as an internal control and expressed as the ratio to WT+Sham (n=3). Values are mean±SEM. *P<0.01 vs WT+Sham; †P<0.01 vs WT+TAC.

TABLE 1. Echocardiographic Data

Variable	WT+Sham (n=6)	KO+Sham (n=6)	WT+TAC (n=9)	KO+TAC (n=10)
Heart rate, bpm	469±10	467±13	475±8	470±6
LV EDD, mm	3.6±0.1	3.6±0.1	3.7±0.1	3.6±0.1
LV ESD, mm	2.2±0.1	2.2±0.1	2.4±0.1	2.3±0.1
Fractional shortening, %	37.2±0.8	36.3±1.0	35.1±0.9	35.5±0.7
Anterior wall thickness, mm	0.70±0.03	0.70±0.03	0.99±0.02*†	0.84±0.03*‡
Posterior wall thickness, mm	0.77±0.02	0.78±0.02	1.04±0.02*†	0.92±0.03*‡

Sham indicates sham operation without ligation of the aorta. Values are mean±SEM.

* $P<0.01$ vs WT+Sham; † $P<0.01$ vs KO+Sham; ‡ $P<0.01$ vs WT+TAC.

Organ Weights

In agreement with echocardiographic LV mass (Figure 3), TAC increased LV weight in WT mice (Figure 4A). Furthermore, in accordance with LV EDP, lung weight/body weight, indicative of pulmonary congestion, increased significantly in WT+TAC (Figure 4B). In KO+TAC, both increased LV and lung weights were significantly reduced.

Histopathology

Masson's trichrome staining showed the increase in myocyte size and interstitial collagen volume fraction in WT+TAC mice compared with WT+Sham mice (Figure 5). The selective disruption of the MMP 2 gene significantly ameliorated myocyte hypertrophy and interstitial fibrosis by TAC. Similarly, picrosirius staining also demonstrated collagen deposition in the interstitial areas in LV sections from WT+TAC mice and the amelioration of interstitial fibrosis in KO+TAC mice (data not shown).

Discussion

In the present study, we demonstrated that the selective disruption of the MMP 2 gene ameliorated LV remodeling, such as myocyte hypertrophy and interstitial fibrosis in TAC

mice, thus providing direct evidence that MMP 2 is involved in mediating PO-induced cardiac hypertrophy. These beneficial effects of MMP 2 inhibition occurred without affecting hemodynamics.

Upregulation of MMP 2 in PO Hypertrophy

The present study demonstrated that the MMP 2 gene expression and gelatinolytic activities were upregulated in the myocardium during PO (Figures 1 and 2). These findings, coupled with past reports, suggest that an increase in myocardial MMP levels is a fairly uniform event in myocardial remodeling.^{2,3,6,19,20} Although the mechanisms responsible for this activation remain to be determined, cellular constituents of cardiac muscle, including fibroblasts, inflammatory cells, and myocytes, are known to be capable of expressing MMP 2 in response to specific stimuli, including mechanical stress.^{9,21}

Role of MMP 2 in PO Hypertrophy

Alterations in the expression and activity of MMP 2 have been demonstrated in a number of pathophysiological conditions, such as myocardial infarction (MI) and heart failure. Our previous study¹⁰ and a recent study by Matsumura et al²² have demonstrated that the inhibition of MMP 2 activity improves the survival rate after acute MI by preventing cardiac rupture and delays after MI remodeling. A recent study by Wang et al²³ has shown that cardiac-specific, constitutively active MMP 2 expression leads to impaired contraction and diminished responses to inotropic stimulation, indicating that MMP 2 can directly impair cardiac function in the absence of superimposed injury.

Broad-spectrum pharmacological inhibition of MMPs significantly attenuated myocardial remodeling associated with chronic volume overload⁵ or hypertension.¹⁹ However, the most effective way to evaluate the contribution of the specific MMP and to obtain the direct evidence for a role of MMP in myocardial remodeling and failure is through such gene manipulation as that used in the present study. As expected, no MMP 2 expression was observed in the myocardium from KO mice in this study (Figures 1 and 2). Thus, the present study could investigate the effects of selective disruption of the MMP 2 gene on the development of myocardial hypertrophy induced by PO.

The most striking finding of the present study was the inhibition of myocardial hypertrophy in MMP 2 KO mice

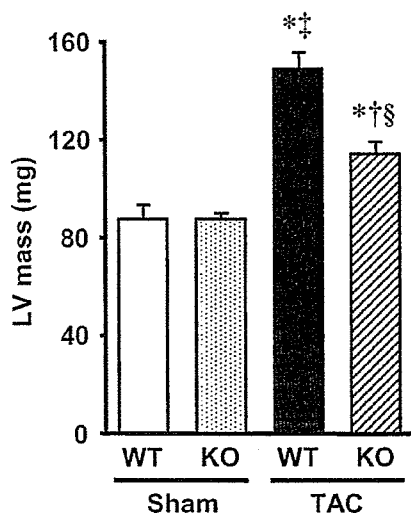


Figure 3. Echocardiographic LV mass from 4 groups of WT+Sham (n=6), KO+Sham (n=6), WT+TAC (n=9), and KO+TAC (n=10) mice. Values are mean±SEM. * $P<0.01$ vs WT+Sham; † $P<0.05$; ‡ $P<0.01$ vs KO+Sham; § $P<0.01$ vs WT+TAC.

TABLE 2. Hemodynamic Data

Variable	WT+Sham (n=6)	KO+Sham (n=6)	WT+TAC (n=9)	KO+TAC (n=10)
Heart rate, bpm	503±3	504±5	507±6	512±6
Arterial blood pressure, mm Hg	73±2	76±5	74±2	71±2
LV systolic pressure, mm Hg	104±4	104±3	202±6*†	196±9*†
LVEDP, mm Hg	1.5±1.2	2.4±0.9	9.8±2.2*†	3.5±0.7‡

Sham indicates sham operation without ligation of the aorta. Values are mean±SEM.

* $P<0.01$ vs WT+Sham; † $P<0.01$ vs KO+Sham; ‡ $P<0.05$ vs WT+TAC.

under PO (Figures 3 through 5). Our previous studies demonstrated the beneficial effects of MMP 2 deletion also on postinfarct LV remodeling and failure.¹⁰ Similar to the present study, both myocyte hypertrophy and interstitial collagen accumulation were ameliorated in the MMP 2-deficient mice after MI. Moreover, the present study is consistent with previous studies from other laboratories, which demonstrated the involvement of myocardial MMP in heart failure.^{2,24,25} Therefore, the present study builds on these past reports by demonstrating that MMP inhibition attenuated myocardial remodeling that occurred also under PO.

The present study demonstrated that increased MMP 2 activity was associated with the interstitial fibrosis in pressure-overloaded LV and the selective inhibition of MMP 2, indeed, ameliorated these changes (Figure 5). Theoretically, an increase in MMP activity would result in a decrease in the MMP substrate, collagens, whereas an inhibition of MMP would result in an increase in collagens. However, in agreement with previous studies,¹⁰ an increase in MMP 2 activity was accompanied by increased fibrosis in our model of LV hypertrophy, which is probably because of the direct proteolysis of myocardial matrix components, as well as by facilitating a profibrotic response. In fact, the selective disruption of the MMP 2 gene did attenuate interstitial fibrosis. Although the present study could not provide the definite explanation for these paradoxical findings, this might be because of the fact that the total ECM collagen content is a complex function of both synthesis and degradation.

In addition to interstitial fibrosis, myocyte cellular hypertrophy was also ameliorated by the selective blockade of the MMP 2 gene (Figure 5), suggesting that myocardial induction of MMP 2 is involved in the development of myocyte hypertrophy during PO. Recently, Heymans et al⁶ demonstrated that MMP 9 gene inactivation reduced hypertrophic changes in cardiac myocytes during acute PO. These results suggest that there is an intimate link between MMPs and the myocyte hypertrophic process, which might be mediated, at least in part, by the tissue infiltration of inflammatory cells. However, the precise role of MMPs in the development of myocyte hypertrophy has not been fully explored. MMPs may be involved in a complex myocyte-matrix interaction, because the basement membrane components, collagen IV and laminin, are the substrates for MMP 2 and MMP 9.²⁶ Thus, increased MMP 2 activity within the myocardium can contribute to the discontinuity of the basement membrane, thereby disrupting the normal myocyte-matrix interface. The findings that MMP inhibition limited the degree of myocyte hypertrophy raise an issue requiring additional studies.

Limitations

There are several issues to be acknowledged as a limitation in this study. First, although in vivo assessment of LV function with echocardiography is feasible and reproducible in the mouse, it might still be difficult to interpret the indices of LV function. However, our validation study has shown that the intraobserver and interobserver variabilities of our echocar-

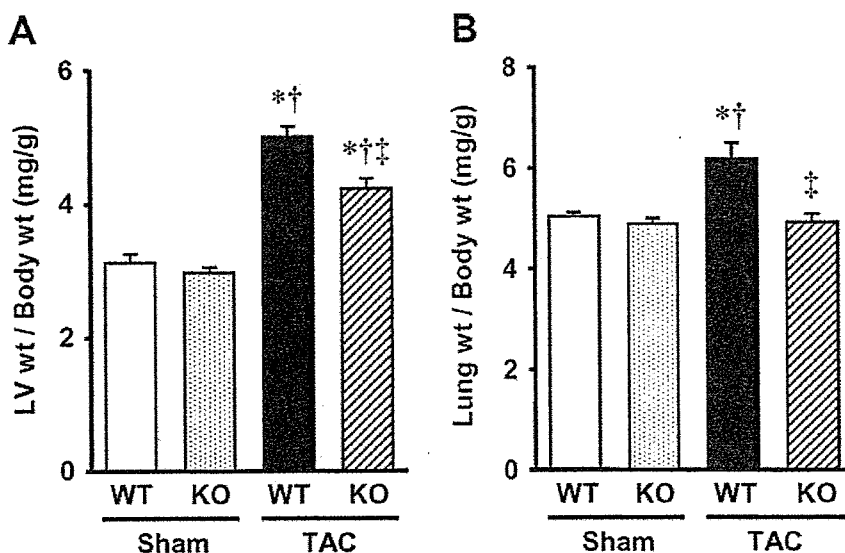


Figure 4. LV weight and lung weight from 4 groups of WT+Sham (n=6), KO+Sham (n=6), WT+TAC (n=9), and KO+TAC (n=10) mice. Values are mean±SEM. * $P<0.01$ vs WT+Sham; † $P<0.01$ vs KO+Sham; ‡ $P<0.01$ vs WT+TAC.

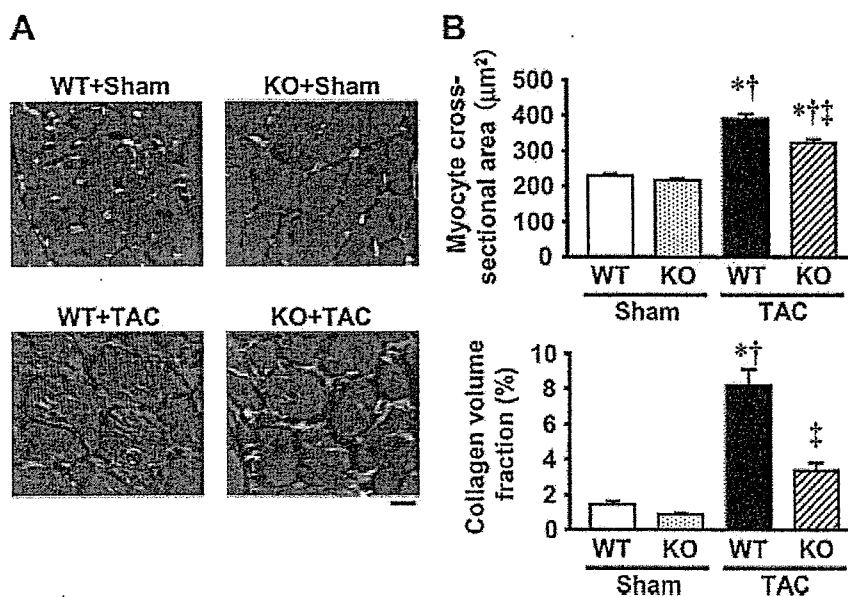


Figure 5. (A) Representative high-power photomicrographs of LV cross-sections stained with Masson's trichrome from 4 groups of WT+Sham, KO+Sham, WT+TAC, and KO+TAC mice. Scale bar, 10 μm. (B) Summary data of myocyte cross-sectional area (top) and collagen volume fraction (bottom) by the histomorphometric analysis of LV tissue sections from 4 groups of WT+Sham (n=4), KO+Sham (n=4), WT+TAC (n=5), and KO+TAC (n=5) mice. Values are mean ± SEM. * $P < 0.01$ vs WT+Sham; † $P < 0.01$ vs KO+Sham; ‡ $P < 0.01$ vs WT+TAC.

diographic measurements for LV dimensions and FS were small, and the measurements made in the same animals on separate days were highly reproducible.¹⁴ Therefore, our technique could be considered to allow for a noninvasive assessment of the LV structure and function. Second, the heart rate values in the present study (460 to 480 bpm) were lower than those (600 bpm) measured in conscious mice. Therefore, the LV size and function data might be greatly influenced by differences in anesthetic regimens and the experimental conditions, such as the heart rate. Third, MMP 9 was not increased in our model of PO hypertrophy. Although the present study could not provide the definite explanation for these results, they might be related to the small number of infiltrating inflammatory cells as neutrophils and macrophages, in which MMP 9 is mainly expressed, within the hypertrophied LV.

Perspectives

Diastolic dysfunction is an important factor contributing to the development of heart failure. One of the most common causes for diastolic heart failure is LV hypertrophy associated with hypertension. The present study demonstrated that MMP 2 inhibition reduced myocyte hypertrophy and interstitial fibrosis, which might contribute to a decrease in LV EDP and lung weight, an index of pulmonary congestion, without affecting LV systolic function. Therefore, although the present study did not directly evaluate the diastolic function itself, the reduction of LV EDP and lung congestion achieved with MMP 2 inhibition in this model is considered to be because of the attenuation of LV hypertrophy and the resultant improvement of diastolic function.

Conclusions

Chronic PO results in an initial cardiac hypertrophic response followed by progressive failure. Our findings provide the first direct evidence that MMP 2 is involved in mediating the adverse myocardial remodeling that occurs in response to a common form of hemodynamic overload. The beneficial

effects of MMP 2 inhibition occurred in the absence of a decrease in systemic blood pressure. These findings suggest that the early institution of MMP 2 inhibition may have use in preventing the development of maladaptive myocardial remodeling in response to hypertension.

Acknowledgments

This study was supported in part by grants from the Ministry of Education, Science and Culture (No. 12670676, 14370230, and 17390223). A part of this study was conducted in Kyushu University Station for Collaborative Research I and II.

References

- Redfield MM, Jacobsen SJ, Burnett JC Jr, Mahoney DW, Bailey KR, Rodeheffer RJ. Burden of systolic and diastolic ventricular dysfunction in the community: appreciating the scope of the heart failure epidemic. *JAMA*. 2003;289:194–202.
- Spinale FG. Matrix metalloproteinases: regulation and dysregulation in the failing heart. *Circ Res*. 2002;90:520–530.
- Peterson JT, Hallak H, Johnson L, Li H, O'Brien PM, Sliksovic DR, Bocan TM, Coker ML, Etoh T, Spinale FG. Matrix metalloproteinase inhibition attenuates left ventricular remodeling and dysfunction in a rat model of progressive heart failure. *Circulation*. 2001;103:2303–2309.
- Sakata Y, Yamamoto K, Mano T, Nishikawa N, Yoshida J, Hori M, Miwa T, Masuyama T. Activation of matrix metalloproteinases precedes left ventricular remodeling in hypertensive heart failure rats: its inhibition as a primary effect of Angiotensin-converting enzyme inhibitor. *Circulation*. 2004;109:2143–2149.
- Polyakova V, Hein S, Kostin S, Ziegelhoeffer T, Schaper J. Matrix metalloproteinases and their tissue inhibitors in pressure-overloaded human myocardium during heart failure progression. *J Am Coll Cardiol*. 2004;44:1609–1618.
- Heymans S, Lupu F, Terclavers S, Vanwetswinkel B, Herbert JM, Baker A, Collen D, Carmeliet P, Moons L. Loss or inhibition of uPA or MMP-9 attenuates LV remodeling and dysfunction after acute pressure overload in mice. *Am J Pathol*. 2005;166:15–25.
- Romanic AM, Harrison SM, Bao W, Burns-Kurtis CL, Pickering S, Gu J, Grau E, Mao J, Sathé GM, Ohlstein EH, Yue TL. Myocardial protection from ischemia/reperfusion injury by targeted deletion of matrix metalloproteinase-9. *Cardiovasc Res*. 2002;54:549–558.
- Cheung PY, Sawicki G, Wozniak M, Wang W, Radomski MW, Schulz R. Matrix metalloproteinase-2 contributes to ischemia-reperfusion injury in the heart. *Circulation*. 2000;101:1833–1839.
- Schubert A, Walther T, Falk V, Binner C, Loscher N, Kanev A, Bleiziffer S, Rauch T, Autschbach R, Mohr FW. Extracellular matrix gene expression correlates to left ventricular mass index after surgical

- induction of left ventricular hypertrophy. *Basic Res Cardiol.* 2001;96:381–387.
10. Hayashidani S, Tsutsui H, Ikeuchi M, Shiomi T, Matsusaka H, Kubota T, Imanaka-Yoshida K, Itoh T, Takeshita A. Targeted deletion of MMP-2 attenuates early LV rupture and late remodeling after experimental myocardial infarction. *Am J Physiol Heart Circ Physiol.* 2003;285:H1229–H1235.
 11. Itoh T, Ikeda T, Gomi H, Nakao S, Suzuki T, Itobara S. Unaltered secretion of β -amyloid precursor protein in gelatinase A (matrix metalloproteinase 2)-deficient mice. *J Biol Chem.* 1997;272:22389–22392.
 12. Rockman HA, Ross RS, Harris AN, Knowlton KU, Steinhilber ME, Field LJ, Ross J Jr, Chien KR. Segregation of atrial-specific and inducible expression of an atrial natriuretic factor transgene in an in vivo murine model of cardiac hypertrophy. *Proc Natl Acad Sci USA.* 1991;88:8277–8281.
 13. Matsusaka H, Ikeuchi M, Matsushima S, Ide T, Kubota T, Feldman AM, Takeshita A, Sunagawa K, Tsutsui H. Selective disruption of MMP-2 gene exacerbates myocardial inflammation and dysfunction in mice with cytokine-induced cardiomyopathy. *Am J Physiol Heart Circ Physiol.* 2005;289:H1858–H1864.
 14. Shiomi T, Tsutsui H, Hayashidani S, Suematsu N, Ikeuchi M, Wen J, Ishibashi M, Kubota T, Egashira K, Takeshita A. Pioglitazone, a peroxisome proliferator-activated receptor- γ agonist, attenuates left ventricular remodeling and failure after experimental myocardial infarction. *Circulation.* 2002;106:3126–3132.
 15. Liao Y, Ishikura F, Beppu S, Asakura M, Takashima S, Asanuma H, Sanada S, Kim J, Ogita H, Kuzuya T, Node K, Kitakaze M, Hori M. Echocardiographic assessment of LV hypertrophy and function in aortic-banded mice: necropsy validation. *Am J Physiol Heart Circ Physiol.* 2002;282:H1703–H1708.
 16. Krege JH, Hodgins JB, Hagaman JR, Smithies O. A noninvasive computerized tail-cuff system for measuring blood pressure in mice. *Hypertension.* 1995;25:1111–1115.
 17. Ishibashi Y, Tsutsui H, Yamamoto S, Takahashi M, Imanaka-Yoshida K, Yoshida T, Urabe Y, Sugimachi M, Takeshita A. Role of microtubules in myocyte contractile dysfunction during cardiac hypertrophy in the rat. *Am J Physiol.* 1996;271:H1978–H1987.
 18. Namba T, Tsutsui H, Tagawa H, Takahashi M, Saito K, Kozai T, Usui M, Imanaka-Yoshida K, Imaizumi T, Takeshita A. Regulation of fibrillar collagen gene expression and protein accumulation in volume-overloaded cardiac hypertrophy. *Circulation.* 1997;95:2448–2454.
 19. Chancey AL, Brower GL, Peterson JT, Janicki JS. Effects of matrix metalloproteinase inhibition on ventricular remodeling due to volume overload. *Circulation.* 2002;105:1983–1988.
 20. Heymans S, Schroen B, Vermeersch P, Milting H, Gao F, Kassner A, Gillijns H, Herijgers P, Flameng W, Carmeliet P, Van de Werf F, Pinto YM, Janssens S. Increased cardiac expression of tissue inhibitor of metalloproteinase-1 and tissue inhibitor of metalloproteinase-2 is related to cardiac fibrosis and dysfunction in the chronic pressure-overloaded human heart. *Circulation.* 2005;112:1136–1144.
 21. Nagatomo Y, Carabello BA, Coker ML, McDermott PJ, Nemoto S, Hamawaki M, Spinale FG. Differential effects of pressure or volume overload on myocardial MMP levels and inhibitory control. *Am J Physiol Heart Circ Physiol.* 2000;278:H151–H161.
 22. Matsumura S, Iwanaga S, Mochizuki S, Okamoto H, Ogawa S, Okada Y. Targeted deletion or pharmacological inhibition of MMP-2 prevents cardiac rupture after myocardial infarction in mice. *J Clin Invest.* 2005;115:599–609.
 23. Wang GY, Bergman MR, Nguyen AP, Turcato S, Swigart PM, Rodrigo MC, Simpson PC, Karliner JS, Lovett DH, Baker AJ. Cardiac transgenic matrix metalloproteinase-2 expression directly induces impaired contractility. *Cardiovasc Res.* 2006;69:688–696.
 24. Heymans S, Lutun A, Nuyens D, Theilmeier G, Creemers E, Moons L, Dyspersin GD, Cleutjens JP, Shipley M, Angellilo A, Levi M, Nube O, Baker A, Keshet E, Lupu F, Herbert JM, Smits JF, Shapiro SD, Baes M, Borgers M, Collen D, Daemen MJ, Carmeliet P. Inhibition of plasminogen activators or matrix metalloproteinases prevents cardiac rupture but impairs therapeutic angiogenesis and causes cardiac failure. *Nat Med.* 1999;5:1135–1142.
 25. Ducharme A, Frantz S, Aikawa M, Rabkin E, Lindsey M, Rohde LE, Schoen FJ, Kelly RA, Werb Z, Libby P, Lee RT. Targeted deletion of matrix metalloproteinase-9 attenuates left ventricular enlargement and collagen accumulation after experimental myocardial infarction. *J Clin Invest.* 2000;106:55–62.
 26. Nagase H, Woessner JF Jr. Matrix metalloproteinases. *J Biol Chem.* 1999;274:21491–21494.

Performance of Super-Orthogonal Convolutional Coding for Ultra-Wideband Systems in Multipath and Multiuser Channels

TOMOKO MATSUMOTO and RYUJI KOHNO

Division of Physics, Electrical and Computer Engineering, Graduate School of Engineering, Yokohama National University, 79-5 Tokiwadai, Hodogaya-ku, Yokohama 240-8501, Japan

E-mail: tomoko@kohnolab.dnj.ynu.ac.jp

Abstract. This paper investigates the application of super-orthogonal convolutional codes (SOCC) to a direct-sequence based ultra-wideband (DS-UWB) system under a realistic environment including inter-symbol interference (ISI) and multiuser interference (MUI). The effect of MUI and ISI on the performance of SOCC is analyzed by using both maximum ratio combining (MRC) RAKE receiver and minimum mean-squared error (MMSE) RAKE receiver followed by matched filter receiver. The analysis shows that in the case of employing simple MRC-RAKE receiver, the performance of SOCC is affected by MUI and ISI because of the short length of the spreading sequence. In order to combat MUI and ISI, a code-hopping scheme is proposed in conjunction with SOCC. The results show that SOCC scheme outperforms the higher-rate conventional convolutional coded scheme for multipath and multiple access channels. Furthermore, the use of MMSE-RAKE receiver to suppress interference is analyzed and the subsequent increase of the system capacity is observed.

Keywords: ultra-wideband communications, super-orthogonal convolutional codes, code-spreading, RAKE receiver

Abbreviations: KAP – Kluwer Academic Publishers; compuscript – Electronically submitted article

1. Introduction

In recent years, ultra-wideband (UWB) technology has received considerable attention. UWB technology has some attractive features including high-data rate, multipath robustness, low cost, and low-power consumption. High-data rate wireless personal area network (HR-WPAN) is one of the applications of UWB technology. Another application is low-data rate WPAN (LR-WPAN), which provides relatively low-data rate transmission over medium range, combined with precise ranging and positioning capabilities.

Due to the large bandwidth, however, it is inevitable for UWB systems to coexist with other existing radio systems. In order to reduce the intra-system interference (ISI), UWB devices must meet stringent power spectral density requirements specified by regulations. This highlights the importance of power efficiency in the design of UWB systems. Therefore, applying strong forward error control codes (FEC) is necessary in order to minimize the impact of power limitation.

In wideband transmissions, very low-rate channel codes are used in conjunction with spreading (referred to as code-spreading), since the bandwidth expansion by error control coding can be utilized as a spreading gain. So far, this code-spreading has been considered

in spread-spectrum systems [1–4]. It is well known that the appropriate allocation of the total bandwidth expansion between coding and spreading can drastically increase the capacity of such wideband systems.

For this reason, the low-rate codes can possibly be applied to UWB system as well, with its spread-spectrum nature [5]. Furthermore, with its wider bandwidth as opposed to the spread-spectrum systems, UWB systems can employ very low-rate codes lower than those used in conventional spread-spectrum systems.

Among the low-rate channel codes, the super-orthogonal convolutional codes (SOCC) introduced in [1], are focused here. So far, the application of SOCC to a time-hopping-based UWB (TH-UWB) has been investigated under multiuser additive white Gaussian noise (AWGN) channel [6] and Rayleigh fading channel [7]. However, in [6,7], neither comparison between SOCC and other channel codes nor performance analysis under realistic UWB multipath fading channel have been achieved.

In this paper, the achievable performance of super-orthogonal (SO) convolutional coded UWB system in a realistic multipath fading channel proposed by IEEE 802.15.3 TG3a [8] is analyzed. The main reason for using SOCC is their near optimal performance and relatively low implementation complexity. In [9], Turbo code and low-density parity check (LDPC) code are applied to UWB system. In this paper, neither turbo nor LDPC code is considered because they increase decoding complexity and delay. It is obvious that our analysis is applicable when it is coupled with turbo coding. The problem in using SOCC for UWB transmission is that when one employs low-rate codes under the constraint where the total spreading factor is fixed, the length of the spreading sequence is shortened, yielding poor auto- and cross-correlation property among spreading codes. This leads to serious multi-user interference (MUI) and ISI. In order to combat such a poor correlation property of the spreading code, there are mainly two strategies, namely, random scrambling [10] and code-hopping. The code-hopping scheme with predetermined multiple sequence is employed in this paper, whereby it leads different interference from symbol to symbol and makes the interference probability density function from other users close to the Gaussian distribution. The performance of the SO coded schemes are compared with the conventional higher rate convolutional coded schemes for two different types of coherent RAKE receiver followed by matched filter, i.e., conventional maximum ratio combining (MRC) receiver and minimum mean squared error (MMSE) combining receiver. The latter type of receiver effectively combines multipath and suppress both MUI and ISI. Furthermore, it can work without knowledge of other user's information, including spreading sequence, received timing and channel impulse response, and so on. Instead, it utilizes the cyclostationarity of interference signals so that it is adopted to the code-hopping scheme. Our performance analysis shows that the SO coded scheme combined with the code-hopping scheme outperforms the conventional higher rate convolutional coded scheme under multipath and multiuser environment for both types of receivers. The organization of this paper is as follows. Section 2 gives the system model. In Section 3, the optimum combining weight of MRC and MMSE RAKE receiver and theoretical upper bound of the bit error rate (BER) are derived. In Section 4, the analysis is confirmed by computer simulations. Finally, in Section 5, conclusions are drawn.

2. System Description

In this section, after briefly describing the encoder and decoder structure of SOCC, the overall system model is described.